might change the function of synaptic vesicle in the hippocampus of AD.

Spot no. 18 was identified as clathrin, which is known as the major protein of the polyhedral coat of coated pits and vesicles [7]. The amount of spot no. 18 was significantly decreased. APP was associated clusters of clathrin-coated vesicles and endosomes [3]. Thus, Aβ oligomers might inhibit the vesicle formation by clathrin.

In addition, we performed a validation experiment for HSP60, NFL, clathrin, Pacsin 1 and β-actin as the altered proteins, and VDAC as the unchanged protein (as control) [23]. The increased levels of clathrin, the decreased levels of HSP60, NFL, and Pacsin 1 and the unchanged level of β-actin and VDAC in $APP_{E693\Delta}$-transgenic mice hippocampus were validated by Western blotting (Fig. 2).

In summary, we identified the altered levels of 14 proteins in $APP_{E693\Delta}$-transgenic mice hippocampus using 2D-DIGE and LC–MS/MS approach. This approach elucidated the pathological effects of Aβ oligomers on hippocampus. Our findings might provide a clue for investigation of the hippocampus of AD early stage.

Acknowledgements

This work was supported by grants from Kobe Gakuin University for Collaborative Research C and the Smoking Research Foundation. The authors thank Dr. Tadanori Mayumi for his encouragement during the early days of the study.

References

[1] U. Andersson, H. Antonicka, J. Houstek, B. Cannon, A novel principle for conferring selectivity to poly(A)-binding proteins: interdependence of two ATP synthase beta-subunit mRNA-binding proteins, Biochemical Journal 346 (Pt 1) (2000) 33–39.
[2] C.L. Chien, R.K. Liem, Characterization of the mouse gene encoding the neuronal intermediate filament protein alpha-internexin, Gene 149 (1994) 289–292.
[3] A. Ferreira, A. Caceres, K.S. Kosik, Intraneuronal compartments of the amyloid precursor protein, Journal of Neuroscience 13 (1993) 3112–3123.
[4] T.A. Fulga, I. Elson-Schwab, V. Khurana, M.L. Steinhilb, T.L. Spires, B.T. Hyman, M.B. Feany, Abnormal bundling and accumulation of F-actin mediates tau-induced neuronal degeneration in vivo, Nature Cell Biology 9 (2007) 139–148.
[5] A. Gorg, C. Obermaier, G. Boguth, A. Harder, B. Scheibe, R. Wildgruber, W. Weiss, The current state of two-dimensional electrophoresis with immobilized pH gradients, Electrophoresis 21 (2000) 1037–1053.
[6] J. Hardy, D.J. Selkoe, The amyloid hypothesis of Alzheimer's disease: progress and problems on the road to therapeutics, Science 297 (2002) 353–356.
[7] J. Hirst, M.S. Robinson, Clathrin and adaptors, Biochimica et Biophysica Acta 1404 (1998) 173–193.
[8] C.R. Hunt, A.J. Parsian, P.C. Goswami, C.A. Kozak, Characterization and expression of the mouse Hsc70 gene, Biochimica et Biophysica Acta 1444 (1999) 315–325.
[9] S. Ikawa, R.A. Weinberg, An interaction between p21ras and heat shock protein hsp60, a chaperonin, Proceedings of the National Academy of Sciences 89 (1992) 2012–2016.
[10] J.L. Johnson, A. Halas, G. Flom, Nucleotide-dependent interaction of Saccharomyces cerevisiae Hsp90 with the cochaperone proteins Sti1, Cpr6, and Sba1, Molecular and Cellular Biology 27 (2007) 768–776.
[11] M. Kaghad, X. Dumont, P. Chalon, J.M. Lelias, N. Lamande, M. Lucas, M. Lazar, D. Caput, Nucleotide sequences of cDNAs alpha and gamma enolase mRNAs from mouse brain, Nucleic Acids Research 18 (1990) 3638.
[12] B.L. Kelly, R. Vassar, A. Ferreira, Beta-amyloid-induced dynamin 1 depletion in hippocampal neurons. A potential mechanism for early cognitive decline in Alzheimer disease, Journal of Biological Chemistry 280 (2005) 31746–31753.
[13] W.L. Klein, G.A. Krafft, C.E. Finch, Targeting small Abeta oligomers: the solution to an Alzheimer's disease conundrum? Trends in Neurosciences 24 (2001) 219–224.
[14] T.B. Kuhn, P.J. Meberg, M.D. Brown, B.W. Bernstein, L.S. Minamide, J.R. Jensen, K. Okada, E.A. Soda, J.R. Bamburg, Regulating actin dynamics in neuronal growth cones by ADF/cofilin and rho family GTPases, Journal of Neurobiology 44 (2000) 126–144.
[15] V.M. Lee, M. Goedert, J.Q. Trojanowski, Neurodegenerative tauopathies, Annual Review of Neuroscience 24 (2001) 1121–1159.
[16] S. Li, S. Hong, N.E. Shepardson, D.M. Walsh, G.M. Shankar, D. Selkoe, Soluble oligomers of amyloid Beta protein facilitate hippocampal long-term depression by disrupting neuronal glutamate uptake, Neuron 62 (2009) 788–801.
[17] J. Modregger, B. Ritter, B. Witter, M. Paulsson, M. Plomann, All three PACSIN isoforms bind to endocytic proteins and inhibit endocytosis, Journal of Cell Science 113 (Pt 24) (2000) 4511–4521.
[18] R.A. Nixon, R.K. Sihag, Neurofilament phosphorylation: a new look at regulation and function, Trends in Neurosciences 14 (1991) 501–506.
[19] R.A. Robinson, M.B. Lange, R. Sultana, V. Galvan, J. Fombonne, O. Gorostiza, J. Zhang, G. Warrier, J. Cai, W.M. Pierce, D.E. Bredesen, D.A. Butterfield, Differential expression and redox proteomics analyses of an Alzheimer disease transgenic mouse model: effects of the amyloid-beta peptide of amyloid precursor protein, Neuroscience 177 (2011) 207–222.
[20] D.J. Selkoe, Alzheimer's disease is a synaptic failure, Science 298 (2002) 789–791.
[21] S.J. Shin, S.E. Lee, J.H. Boo, M. Kim, Y.D. Yoon, S.I. Kim, I. Mook-Jung, Profiling proteins related to amyloid deposited brain of Tg2576 mice, Proteomics 4 (2004) 3359–3368.
[22] R. Sultana, D. Boyd-Kimball, J. Cai, W.M. Pierce, J.B. Klein, M. Merchant, D.A. Butterfield, Proteomics analysis of the Alzheimer's disease hippocampal proteome, Journal of Alzheimer's Disease 11 (2007) 153–164.
[23] M. Takano, K. Maekura, M. Otani, K. Sano, T. Nakamura-Hirota, S. Tokuyama, K.S. Min, T. Tomiyama, H. Mori, S. Matsuyama, Proteomic analysis of the brain tissues from a transgenic mouse model of amyloid beta oligomers, Neurochemistry International 61 (2012) 347–355.
[24] M. Takano, M. Otani, A. Sakai, K. Kadoyama, S. Matsuyama, A. Matsumoto, M. Takenokuchi, M. Sumida, T. Taniguchi, Use of a phosphosensor dye in proteomic analysis of human mutant tau transgenic mice, Neuroreport 20 (2009) 1648–1653.
[25] T. Tomiyama, S. Matsuyama, H. Iso, T. Umeda, H. Takuma, K. Ohnishi, K. Ishibashi, R. Teraoka, N. Sakama, T. Yamashita, K. Nishitsuji, K. Ito, H. Shimada, M.P. Lambert, W.L. Klein, H. Mori, A mouse model of amyloid beta oligomers: their contribution to synaptic alteration, abnormal tau phosphorylation, glial activation, and neuronal loss in vivo, Journal of Neuroscience 30 (2010) 4845–4856.

Biochemical and Biophysical Research Communications 421 (2012) 140–144

Contents lists available at SciVerse ScienceDirect

Biochemical and Biophysical Research Communications

journal homepage: www.elsevier.com/locate/ybbrc

Annexin A4 is a possible biomarker for cisplatin susceptibility of malignant mesothelioma cells

Takuya Yamashita [a,b,1], Kazuya Nagano [a,1], So-ichiro Kanasaki [a,b], Yuka Maeda [a,b], Takeshi Furuya [a,b], Masaki Inoue [a], Hiromi Nabeshi [b], Tomoaki Yoshikawa [a,b], Yasuo Yoshioka [a,b,c], Norio Itoh [b], Yasuhiro Abe [a], Haruhiko Kamada [a,c], Yasuo Tsutsumi [a,b,c], Shin-ichi Tsunoda [a,c,d,*]

[a] Laboratory of Biopharmaceutical Research, National Institute of Biomedical Innovation, 7-6-8 Saito-Asagi, Ibaraki, Osaka 567-0085, Japan
[b] Laboratory of Toxicology and Safety Science, Graduate School of Pharmaceutical Sciences, Osaka University, 1-6 Yamadaoka, Suita, Osaka 565-0871, Japan
[c] The Center for Advanced Medical Engineering and Informatics, Osaka University, 1-6 Yamadaoka, Suita, Osaka 565-0871, Japan
[d] Laboratory of Biomedical Innovation, Graduate School of Pharmaceutical Sciences, Osaka University, 1-6 Yamadaoka, Suita, Osaka 565-0871, Japan

ARTICLE INFO

Article history:
Received 27 March 2012
Available online 4 April 2012

Keywords:
Malignant mesothelioma
Cisplatin susceptibility
Annexin A4
Biomarker
Proteomics

ABSTRACT

Mesothelioma is a highly malignant tumor with a poor prognosis and limited treatment options. Although cisplatin (CDDP) is an effective anticancer drug, its response rate is only 20%. Therefore, discovery of biomarkers is desirable to distinguish the CDDP-susceptible versus resistant cases. To this end, differential proteome analysis was performed to distinguish between mesothelioma cells of different CDDP susceptibilities, and this revealed that expression of annexin A4 (ANXA4) protein was higher in CDDP-resistant cells than in CDDP-susceptible cells. Furthermore, ANXA4 expression levels were higher in human clinical malignant mesothelioma tissues than in benign mesothelioma and normal mesothelial tissues. Finally, increased susceptibility was observed following gene knockdown of ANXA4 in mesothelioma cells, whereas the opposite effect was observed following transfection of an ANXA4 plasmid. These results suggest that ANXA4 has a regulatory function related to the cisplatin susceptibility of mesothelioma cells and that it could be a biomarker for CDDP susceptibility in pathological diagnoses.

1. Introduction

Malignant mesothelioma is an aggressive neoplasm located on serosal membrane surfaces such as the pleura, and less frequently the peritoneum, and it has a poor outcome. The five-year survival rate is only about 5%. On the other hand, it is well known that asbestos is the major causative agent in the development of this disease [1–3]. Moreover, malignant mesothelioma takes 40–50 years to develop following exposure to asbestos. Because of its adiabatic potential, asbestos was commonly used as a building material in the 1960–1970s. Thus, an increase in mesothelioma patients is expected in the future. Patients with pleural malignant mesothelioma commonly present with an effusion associated with breathlessness that is often accompanied by chest-wall pain and a cough. After confirming the diagnosis, many patients are treated by intensive multidirectional approaches that combine cytoreductive surgery with intrapleural or intraperitoneal chemotherapy [4–8]. However, cytoreductive surgery is not always possible for patients with extensive intraperitoneal disease. Thus, the role of chemotherapy in malignant mesothelioma is critically important.

CDDP is an extensively used anticancer drug for the treatment of malignant mesothelioma, although the response rate is only about 20% [9–12]. A major problem with CDDP treatment of malignant mesothelioma patients is the development of CDDP insusceptibility. Thus, there is an urgent need to further our understanding of the pathogenesis of malignant mesothelioma, particularly with respect to the expression of proteins that confer drug susceptibility, in order to develop novel therapeutic strategies. In this study, a proteomic analysis was performed using high- and low-CDDP-susceptible malignant mesothelioma cells to identify candidate proteins associated with CDDP susceptibility.

2. Materials and methods

2.1. Cells

H28, H2052, H2452, H226 and MSTO-221H were purchased from American Type Culture Collection and maintained in RPMI1640 medium (Wako) containing 10% fetal calf serum (Biowest). Human mesothelial cells (HMC) were purchased from

* Corresponding author at: Laboratory of Biopharmaceutical Research, National Institute of Biomedical Innovation, 7-6-8 Saito-Asagi, Ibaraki, Osaka 567-0085, Japan. Fax: +81 72 641 9817.
E-mail address: tsunoda@nibio.go.jp (S.-i. Tsunoda).
[1] These authors contributed equally to this work.

0006-291X/$ - see front matter © 2012 Elsevier Inc. All rights reserved.
http://dx.doi.org/10.1016/j.bbrc.2012.03.144

Sciencell and cultured in Mesothelial Cell Growth Medium (ZenBio) under a 5% CO_2 atmosphere at 37 °C.

2.2. Measurement of cisplatin susceptibility in malignant mesothelioma cells

Malignant mesothelioma cells were seeded into 96-well microplates and cultured overnight. Various concentrations of CDDP were added to each well, the plates were incubated for 24 h, and cell viability was measured using Cell count reagent SF (Nacalai tesque). Absorbance was measured using a microplate reader (Bio-Rad) at test and reference wavelengths of 450 and 650 nm, respectively.

2.3. Proteomic analysis using two dimensional differential in-gel electrophoresis

For proteomic analysis, quantitative analysis was performed using two dimensional differential in-gel electrophoresis (2D-DIGE). Cell lysates were prepared from H28 and H2052 and then solubilized with 7 M urea, 2 M thiourea, 4% CHAPS and 10 mM Tris–HCl (pH 8.5). The lysates were labeled at the ratio of 50 μg proteins: 400 pmol Cy3 or Cy5 protein-labeling dye (GE Healthcare Biosciences) in dimethylformamide according to the manufacturer's protocol. The labelled samples were mixed with rehydration buffer (7 M urea, 2 M thiourea, 4% CHAPS, 2% DTT, 2% Pharmalyte (GE Healthcare Biosciences)) and applied to a 24-cm immobilized pH gradient gel strip (IPG-strip pH 4–7) for separation in the first dimension. For the second dimension separation, the IPG-strips were treated with iodoacetamide and applied to SDS–PAGE gels (10% polyacrylamide and 2.7% *N,N′*-diallyltartardiamide gels). After electrophoresis, the gels were scanned with a laser fluoroimager (Typhoon Trio, GE Healthcare Biosciences). The spot-picking gel was scanned after staining with Deep purple total protein stain (GE Healthcare Biosciences). Quantitative analysis of protein spots was carried out with Decyder-DIA software (GE Healthcare Biosciences). For the antigen spots of interest, spots of 1 mm × 1 mm in size were picked using Ettan Spot Picker (GE Healthcare Biosciences).

2.4. In-gel tryptic digestion

Picked gel pieces were destained with 50% acetonitrile/50 mM NH_4HCO_3 for 20 min twice, dehydrated with 75% acetonitrile for 20 min, and then dried using a centrifugal concentrator. Five microliter of 20 μg/ml trypsin (Promega) solution was added to each gel piece and the pieces were incubated for 16 h at 37 °C. The digested peptides were extracted sequentially using 50%, 80%, and 100% acetonitrile and then dried before being suspended in 10 μl of 0.1% formic acid.

2.5. Mass spectrometry and database search

Extracted peptides were analyzed by liquid chromatography ultra high resolution time-of-flight mass spectrometry (LC-UHR TOF-MS/MS; maXis, Bruker Daltonics). The Mascot search engine (http://www.matrixscience.com) was initially used to query the entire theoretical tryptic peptide database as well as SwissProt (http://www.expasy.org/, a public domain database provided by the Swiss Institute of Bioinformatics). The search query assumed the following: (i) the peptides were mono-, di- or tri-isotopic, (ii) methionine residues may be oxidized, (iii) all cysteines were modified with carbamidomethyl.

2.6. Western blot

The cell lysates were separated in 10% SDS–polyacrylamide gels and transferred to Immobilon membranes (Millipore). After blocking by 4% block ace (DS Pharma Biomedical) for 1 h at room temperature, the blots were reacted with primary antibodies in a buffer containing 0.4% block ace, and then with the appropriate peroxidase-conjugated secondary antibodies in the same buffer. Expression of ANXA4 in malignant mesothelioma cells was detected by mouse anti-human ANXA4 (Abnova: 1D3) followed by an HRP-conjugated anti-mouse IgG antibody (Sigma–Aldrich) using the ECL-plus system (GE Healthcare Biosciences). Equal amounts of protein loading were confirmed by parallel β-actin immunoblotting, and signal quantification was performed by densitometric scanning.

2.7. Immunohistochemistry staining

Human mesothelioma and normal tissue sections were deparaffinated in xylene and rehydrated in a graded series of ethanol dilutions. Heat-induced epitope retrieval was performed by incubating at different temperatures following the manufacturer's instructions using Target Retrieval Solution pH 9 (Dako). After heat-induced epitope retrieval treatment, endogenous peroxidase was blocked with a peroxidase blocking reagent (Dako). Following peroxidase blocking, the slides were incubated with 10% bovine serum albumin (BSA) solution for 30 min at room temperature. The slides were then incubated for 60 min with anti-human ANXA4 monoclonal antibody (9 μg/ml) in 3% BSA at room temperature. After washing 3 times with wash buffer (Dako), the slides were incubated for 30 min with ENVISION + Dual Link (Dako) at room temperature. They were then washed final 3 times and stained with 3,3′-diaminobenzidine. After development, the slides were lightly counterstained with Mayer's hematoxylin and mounted with resinous mounting medium.

2.8. Cisplatin susceptibility in cells transfected with ANXA4-siRNA and ANXA4-plasmid

H28 was transfected with ANXA4-siRNA (target sequence: AAGGATATCACAGAAGGATAT, Qiagen) using Hyperfect reagent (Qiagen) according to the manufacturer's instructions. In contrast, H2052 was transfected with ANXA4-pcDNA 3.1 (a gift from Naka T: Laboratory for Immune Signal, National Institute of Biomedical Innovation) using FuGENE HD transfection reagent (Roche). After transfection, the cells were treated with various concentrations of CDDP for 36 h (ANXA4-siRNA) or 24 h (ANXA4-pcDNA 3.1). Cell viability was measured as described above.

2.9. Statistical analysis

Differences in tumor volumes between the control and target groups were compared using the unpaired Student's *t*-test.

3. Results

3.1. CDDP susceptibility in malignant mesothelioma cells

Cell viability following CDDP treatment was examined to determine which cell lines had higher or lower susceptibility to CDDP. Among five tested mesothelioma cell lines, H2052 was the most and H28 the least susceptible cell line (Fig. 1). The IC_{50} values of H28, H2052, H2452, H226 and MSTO-221H were 154.5, 27.8, 66.0, 87.5 and 49.5 μM, respectively.

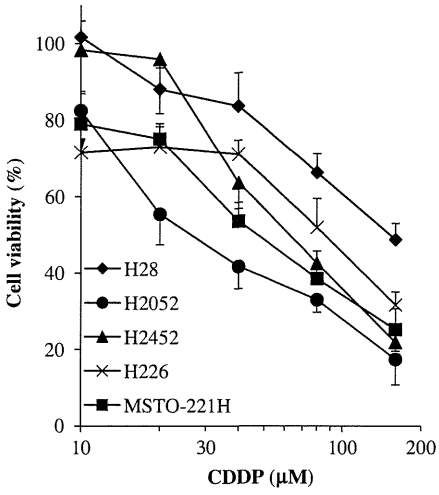

Fig. 1. Susceptibility of malignant mesothelioma cells to CDDP. Mesothelioma cells, H28, H2052, H2452, H226 and MSTO-221H were cultured with various concentrations of CDDP for 24 h 37 °C under 5% CO_2. Cell viability was assayed using the WST-8 assay. Maximal cell viability (100%) was obtained by incubating cells without CDDP. Data are shown as means and standard deviations ($n = 4$).

3.2. Identification of differentially expressed proteins by 2D-DIGE and MS

In order to search for CDDP susceptibility-related proteins, differential proteome analysis between H2052 and H28 cell lines was performed to search for CDDP susceptibility-related proteins (Fig. 2). Quantitative image analysis indicated that a total of eight protein spots representing > 2.0-fold alteration in expression were found and then identified by MS analysis (Table 1). Among those eight proteins, we focused on ANXA4 because this protein plays an important role in membrane stability. Previous reports have indicated that ANXA4 is associated with chemoresistance against platinum-based anticancer drugs in human lung, colon [13] and ovarian cancer [14].

3.3. ANXA4 expression analysis in human malignant mesothelioma cells and mesothelial tissues

Correlations between the expression levels in five malignant mesothelioma cell lines with CDDP-susceptibility were examined using western blot analysis to validate the identified proteins as CDDP susceptibility-related proteins. ANXA4 was expressed at a higher level in H28 cells relative to the other four CDDP-susceptible malignant mesothelioma cell lines (Fig. 3A and B). Expression of ANXA4 in human mesothelial tissue was analyzed by immunohistochemistry staining with an anti-human ANXA4 monoclonal antibody. Fig. 3C indicates that ANXA4 was expressed at higher levels in human malignant mesothelioma tissues than in benign mesothelioma tissues and normal mesothelial tissues.

3.4. Gene regulation of ANXA4 in malignant mesothelioma cells by knockdown and overexpression

ANXA4-siRNA and ANXA4-pcDNA 3.1 were next transfected to H28 and H2052 before CDDP treatment to evaluate correlations between ANXA4 expression levels and CDDP susceptibility. The IC_{50} values of [H28/non treat: H28/control-siRNA: H28/ANXA4-siRNA] were [80.0 μM: 71.8 μM: 15.5 μM] and [H2052/control-pcDNA 3.1: [H2052/ANXA4-pcDNA 3.1] were [55.2 μM: 89.7 μM], respectively (Fig. 4A–D). These results suggested that the CDDP susceptibility of H28 cells was increased by ANXA4-siRNA transfection and that of H2052 cells was decreased by ANXA4-pcDNA 3.1 transfection.

4. Discussion

In this study, a proteomic analysis was performed based on 2D-DIGE using malignant mesothelioma cell lines to identify candidate proteins associated with CDDP susceptibility (Figs. 1 and 2). Eight proteins that were differentially expressed in H28 cells compared with H2052 cells were identified (Table 1). ANXA4 was found to be expressed at a higher level in H28 cells relative to levels in CDDP-susceptible malignant mesothelioma cells by western blot

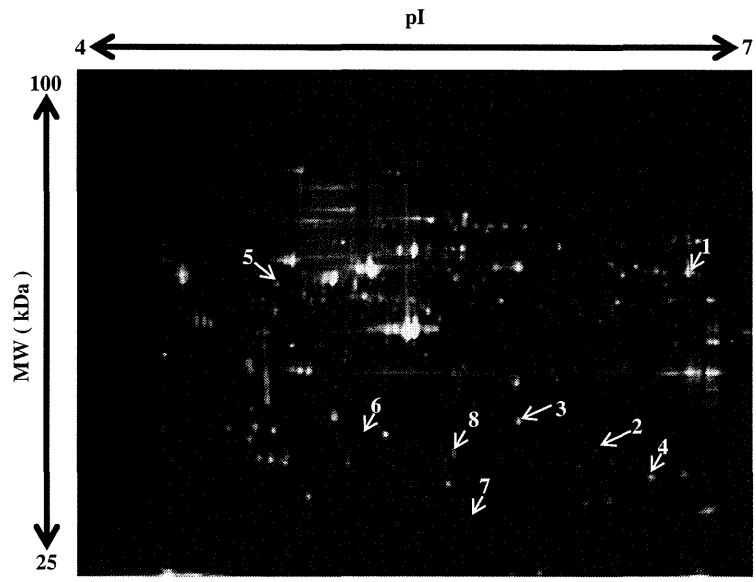

Fig. 2. 2D-DIGE image of fluorescently labeled proteins from human mesothelioma cell lines H28 and H2052. Proteins from high- and low-susceptible mesothelioma cells (H2052, H28) were labeled with cy3 and cy5, respectively, and 2D electrophoresis was performed. The differentially expressed spots in H28 indicated by white arrows were then identified by LC-TOF-MS/MS. Table 1 contains additional information about the identified proteins.

Table 1
Proteins expressed at higher or lower levels in H28 compared to H2052.

No.	Accession number	Protein name	pI	MW (kDa)	Expression ratio (H28/H2052)
1	P11413	Glucose-6-phosphate 1-dehydrogenase	6.4	59.3	21.0
2	P78417	Glutathione *S*-transferase omega-1	6.2	27.6	7.4
3	P09525	Annexin A4	5.6	35.9	3.6
4	P30041	Peroxiredoxin-6	6.0	25.0	3.5
5	Q09028	Histone-binding protein RBBP4	4.7	47.7	3.0
6	P07195	L-lactate dehydrogenase B chain	5.7	36.6	2.9
7	P32119	Peroxiredoxin-2	5.7	21.9	0.03
8	Q9Y696	Chloride intracellular channel protein 4	5.5	28.8	0.13

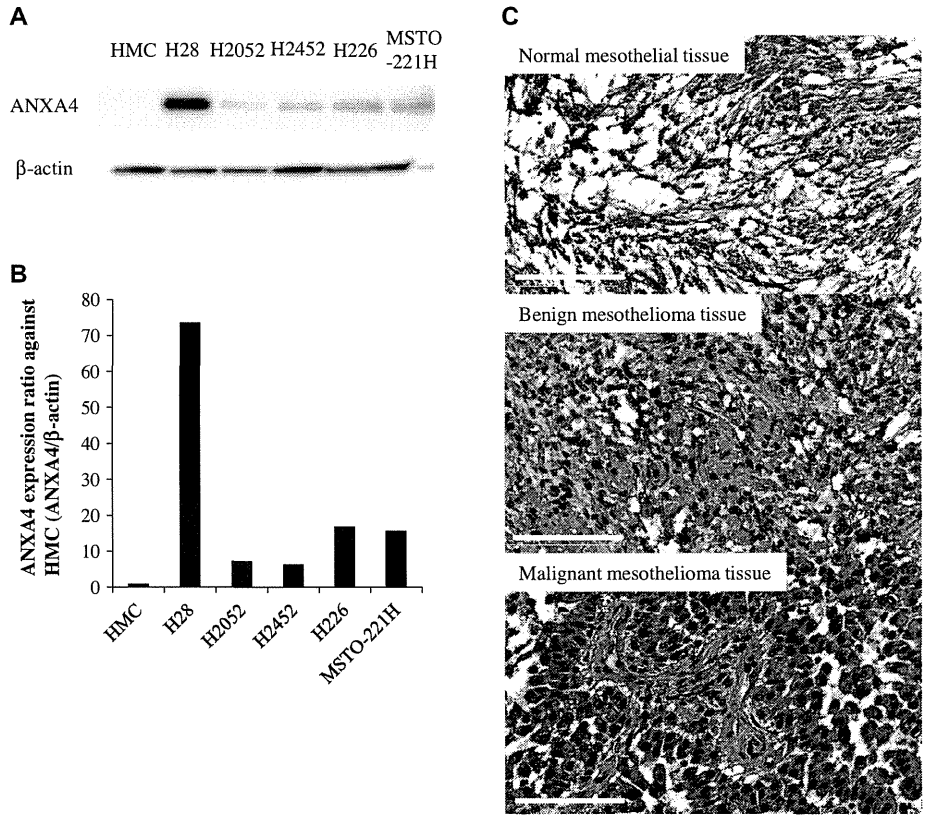

Fig. 3. ANXA4 expression analysis in human malignant mesothelioma cells and mesothelial tissues. ANXA4 expression levels in human primary mesothelial cells, HMC, and mesothelioma cell lines (H28, H2052, H2452, H226, MSTO-221H) were analyzed by western blotting (A). Intensity of the western blotting images was quantified by densitometry (B). Expression of ANXA4 in human mesothelial tissues was analyzed by immunostaining using an anti-human ANXA4 antibody (C). Top, middle and bottom panels are normal mesothelial, benign and malignant mesothelioma tissues, respectively. The tissue sections were counterstained using hematoxylin. Representative 400 × photomicrographs presented (bar: 100 μm).

analysis (Fig. 3A and B). Furthermore, ANXA4 was expressed in malignant mesothelioma tissue but not in benign mesothelial tumor and normal mesothelial tissues (Fig. 3C). Thus, ANXA4 was expressed in CDDP-susceptible malignant mesothelioma cells and specifically in malignant mesothelioma tissues. These results indicate that ANXA4 expression in malignant mesothelioma cells may be correlated with CDDP susceptibility, although this relationship must be validated in future studies of human clinical malignant mesothelial cases. The CDDP susceptibility of H28 cells was actually increased by ANXA4 knockdown, and that of H2052 cells was decreased by ANXA4 overexpression (Fig. 4). Thus, these results suggest that ANXA4 plays an important role in chemoresistance against CDDP.

ANXA4 has already been characterized as a regulator of cell membranes with calcium dependency [15–17]. Recently, some studies have reported the protein is associated with membrane permeability [18], ion channels [19] and exocytosis [20,21]. These observations may explain in part the correlation of ANXA4 with modulation of drug susceptibility in cancer cells.

This study demonstrates for the first time elevated ANXA4 protein expression in malignant mesothelioma cells that have less susceptibility to CDDP. *In vitro* evaluation of drug susceptibility against CDDP in malignant mesothelioma cells derived from cancer patients would be important in clinical conditions because doctors as well as patients wish to avoid treatment with inefficacious drugs. Consequently, the susceptibility of a given patient against CDDP could be confirmed by analyzing the expression level of ANXA4 in malignant mesothelioma patients at the time of diagnosis. Furthermore, if ANXA4 expression could be blocked specifically in malignant mesothelioma cells by nucleic acid drugs such as siRNA, this procedure would prove useful in clinical situations involving CDDP treatment. The present study may contribute to

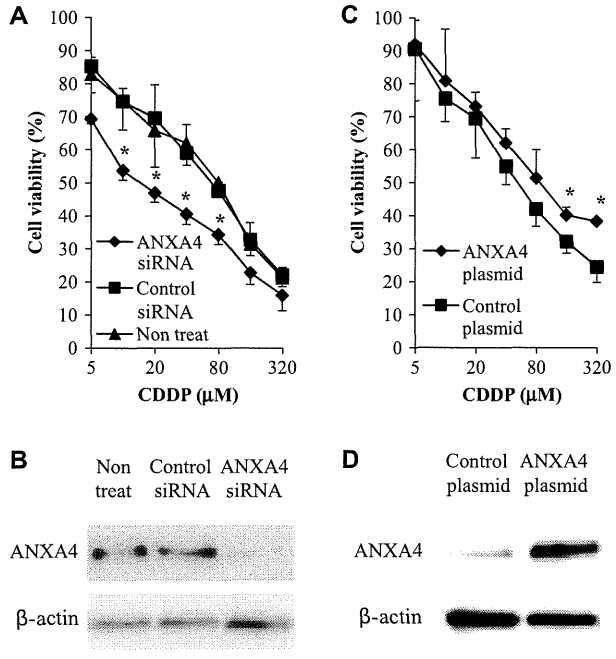

Fig. 4. The effect of ANXA4 gene knockdown and overexpression on CDDP susceptibility in malignant mesothelioma cells. Transfection of ANXA4 siRNA or plasmid into malignant mesothelioma cells confers resistance to CDDP. Cell survival after 24 h treatment of H28/ANXA4 siRNA or H2052/ANXA4 plasmid with different concentrations of CDDP (A and C). Expression of ANXA4 was analyzed by western blot analysis (B and D). Data are shown as means and standard deviations ($n = 4$). *$P < 0.05$ (Control siRNA or plasmid vs. ANXA4 siRNA or plasmid).

establishment of a new therapeutic strategy for malignant mesothelioma patients by suggesting a novel diagnostic and therapeutic target.

Acknowledgments

This study was supported in part by Grants-in-Aid for Scientific Research from the Ministry of Education, Culture, Sports, Science and Technology of Japan, and from the Japan Society for the Promotion of Science (JSPS). This study was also supported in part by Health Labor Sciences Research Grants from the Ministry of Health, Labor and Welfare of Japan and by Health Sciences Research Grants for Research on Publicly Essential Drugs and Medical Devices from the Japan Health Sciences Foundation.

References

[1] W.N. Rom, W.D. Travis, A.R. Brody, Cellular and molecular basis of the asbestos-related diseases, Am. Rev. Respir. Dis. 143 (1991) 408–422.
[2] N.H. Heintz, Y.M. Janssen-Heininger, B.T. Mossman, Asbestos, lung cancers, and mesotheliomas: from molecular approaches to targeting tumor survival pathways, Am. J. Respir. Cell Mol. Biol. 42 (2010) 133–139.
[3] Consensus Report: Asbestos, asbestosis, and cancer: the Helsinki criteria for diagnosis and attribution. Scand. J. Work Environ. Health 23 (1997) 311–316.
[4] T.D. Yan, L. Welch, D. Black, P.H. Sugarbaker, A systematic review on the efficacy of cytoreductive surgery combined with perioperative intraperitoneal chemotherapy for diffuse malignancy peritoneal mesothelioma, Ann. Oncol. 18 (2007) 827–834.
[5] E. Chailleux, D. Pioche, S. Chopra, G. Dabouis, P. Germaud, A.Y. De Lajartre, M. De Lajartre, Prognostic factors in diffuse malignant pleural mesothelioma: a study of 167 patients, Chest 93 (1988) 159–162.
[6] K.S. Sridhar, R. Doria, W.A. Raub Jr., R.J. Thurer, M. Saldana, New strategies are needed in diffuse malignant mesothelioma, Cancer 70 (1992) 2969–2979.
[7] M. Markman, D. Kelsen, Efficacy of cisplatin-based intraperitoneal chemotherapy as treatment of malignant peritoneal mesothelioma, J. Cancer Res. Clin. Oncol. 118 (1992) 547–550.
[8] G.H. Eltabbakh, M.S. Piver, R.E. Hempling, F.O. Recio, M.E. Intengen, Clinical picture, response to therapy, and survival of women with diffuse malignant peritoneal mesothelioma, J. Surg. Oncol. 70 (1999) 6–12.
[9] T. Berghmans, M. Paesmans, Y. Lalami, I. Louviaux, S. Luce, C. Mascaux, A.P. Meert, J.P. Sculier, Activity of chemotherapy and immunotherapy on malignant mesothelioma: a systematic review of the literature with meta-analysis, Lung. Cancer 38 (2002) 111–121.
[10] H.J. Lerner, D.A. Schoenfeld, A. Martin, G. Falkson, E. Borden, Malignant mesothelioma: The Eastern Cooperative Oncology Group (ECOG) experience, Cancer 52 (1983) 1981–1985.
[11] D.M. Mintzer, D. Kelsen, D. Frimmer, R. Heelan, R. Gralla, Phase II trial of high-dose cisplatin in patients with malignant mesothelioma, Cancer Treat Rep. 69 (1985) 711–712.
[12] B.L. Zidar, S. Green, H.I. Pierce, R.W. Roach, S.P. Balcerzak, L. Militello, A phase II evaluation of cisplatin in unresectable diffuse malignant mesothelioma: a Southwest Oncology Group Study, Invest New Drugs 6 (1988) 223–226.
[13] E.K. Han, S.K. Tahir, S.P. Cherian, N. Collins, S.C. Ng, Modulation of paclitaxel resistance by annexin IV in human cancer cell lines, Br. J. Cancer 83 (2000) 83–88.
[14] A. Kim, T. Enomoto, S. Serada, Y. Ueda, T. Takahashi, B. Ripley, T. Miyatake, M. Fujita, C.M. Lee, K. Morimoto, M. Fujimoto, T. Kimura, T. Naka, Enhanced expression of Annexin A4 in clear cell carcinoma of the ovary and its association with chemoresistance to carboplatin, Int. J. Cancer 125 (2009) 2316–2322.
[15] M.A. Kaetzel, P. Hazarika, J.R. Dedman, Differential tissue expression of three 35-kDa annexin calcium-dependent phospholipid-binding proteins, J. Biol. Chem. 264 (1989) 14463–14470.
[16] G. Zanotti, G. Malpeli, F. Gliubich, C. Folli, M. Stoppini, L. Olivi, A. Savoia, R. Berni, Structure of the trigonal crystal form of bovine annexin IV, Biochem. J. 329 (1998) 101–106.
[17] M.A. Kaetzel, Y.D. Mo, T.R. Mealy, B. Campos, W. Bergsma-Schutter, A. Brisson, J.R. Dedman, B.A. Seaton, Phosphorylation mutants elucidate the mechanism of annexin IV-mediated membrane aggregation, Biochemistry 40 (2001) 4192–4199.
[18] W.G. Hill, M.A. Kaetzel, B.K. Kishore, J.R. Dedman, M.L. Zeidel, Annexin A4 reduces water and proton permeability of model membranes but does not alter aquaporin 2-mediated water transport in isolated endosomes, J. Gen. Physiol. 121 (2003) 413–425.
[19] M.A. Kaetzel, H.C. Chan, W.P. Dubinsky, J.R. Dedman, D.J. Nelson, A role for annexin IV in epithelial cell function. Inhibition of calcium-activated chloride conductance, J. Biol. Chem. 269 (1994) 5297–5302.
[20] H. Sohma, C.E. Creutz, S. Gasa, H. Ohkawa, T. Akino, Y. Kuroki, Differential lipid specificities of the repeated domains of annexin IV, Biochim. Biophys. Acta 1546 (2001) 205–215.
[21] A. Piljic, C. Schultz, Annexin A4 self-association modulates general membrane protein mobility in living cells, Mol. Biol. Cell 17 (2006) 3318–3328.

Laboratory of Biopharmaceutical Research[1], National Institute of Biomedical Innovation; Laboratory of Toxicology and Safety Science[2], Graduate School of Pharmaceutical Sciences; The Center for Advanced Medical Engineering and Informatics[3]; Laboratory of Biomedical Innovation[4], Graduate School of Pharmaceutical Sciences, Osaka University, Osaka, Japan

Rho GDP-dissociation inhibitor alpha is associated with cancer metastasis in colon and prostate cancer

T. YAMASHITA[1,2,*], T. OKAMURA[1,*], K. NAGANO[1,*], S. IMAI[1], Y. ABE[1], H. NABESHI[1,2], T. YOSHIKAWA[1,2], Y. YOSHIOKA[1,2,3], H. KAMADA[1,3], Y. TSUTSUMI[1,2,3], S. TSUNODA[1,3,4]

Received July 7, 2011, accepted August 5, 2011

Shin-ichi Tsunoda, Ph.D, Laboratory of Biopharmaceutical Research, National Institute of Biomedical Innovation, 7-6-8 Saito-Asagi, Ibaraki, Osaka 567-0085, Japan.
tsunoda@nibio.go.jp
**These authors contributed equally to the work.*

Pharmazie 67: 253–255 (2012) *doi: 10.1691/ph.2012.1630*

Since metastasis is one of the most important prognostic factors in colorectal cancer, development of new methods to diagnose and prevent metastasis is highly desirable. However, the molecular mechanisms leading to the metastatic phenotype have not been well elucidated. In this study, a proteomics-based search was carried out for metastasis-related proteins in colorectal cancer by analyzing the differential expression of proteins in primary versus metastasis focus-derived colorectal tumor cells. Protein expression profiles were determined using a tissue microarray (TMA), and the results identified Rho GDP-dissociation inhibitor alpha (Rho GDI) as a metastasis-related protein in colon and prostate cancer patients. Consequently, Rho GDI may be useful as a diagnostic biomarker and/or a therapeutic to prevent colon and prostate cancer metastasis.

1. Introduction

Colorectal cancer is known as a major metastatic cancer, and 40–50% of patients already have a metastatic focus at presentation. Moreover, the 5-year survival of these patients is under 10% (Davies et al. 2005). Thus, metastasis is one of the most important prognostic factors in colorectal cancer. In order to improve rates of cancer remission, it will be necessary to clarify the detailed molecular mechanisms of cancer metastasis and to utilize this information to establish new diagnostic and therapeutic techniques. Many researchers have searched for metastasis-related molecules (Liu et al. 2010; Shuehara et al. 2011) using proteomics techniques (Hanash 2003). Comprehensive mapping of the molecular changes during metastasis would greatly improve our understanding of the recurrence and management of cancer. However, the knowledge gained so far in these studies has not been sufficient to improve cancer remission rates.

Here we show the potential of Rho GDI as a metastasis-related protein in colon and prostate cancer patients. In order to identify metastasis-related proteins, the protein expression patterns of human colorectal cancer cells with different metastatic characters were compared. Because these cells were derived from the same patient (SW480: a surgical specimen of a primary colon adenocarcinoma, SW620: a lymph node metastatic focus), cancer metastasis-related protein candidates could be effectively sought without background variations due to differences between individuals. Furthermore, by analyzing the expression of candidate proteins in many clinical samples using a TMA, we attempted to validate the association of these candidates with metastasis. TMA is a slide glass containing many clinical tissues, and it enables one to carry out a high-throughput analysis by evaluating the relationship between expression profiles of each candidate molecule and clinical information such as metastasis. (Imai et al. 2011; Yoshida et al. 2011).

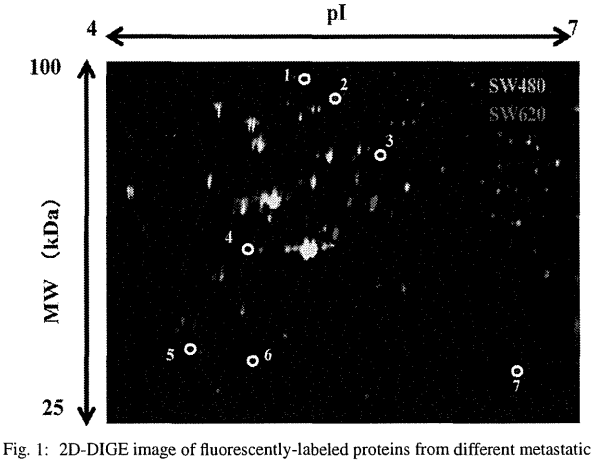

Fig. 1: 2D-DIGE image of fluorescently-labeled proteins from different metastatic human colorectal cancer cells. SW480 is human colorectal cancer cell line derived from a primary tumor and SW620 is derived from a metastatic focus from the same patient. Proteins from the colon cancer cells (SW480, SW620) were labeled with Cy3 and Cy5 respectively, and analyzed by 2D electrophoresis. The differentially-expressed spots (white circles) were then identified by LC-UHR TOF/MS

Table 1: High expression proteins in SW620 compared to SW480

	Accession	Protein name	MW (kDa)	pI	Ratio (SW620 / SW480)
1	P12109	collagen alpha-1(VI) chain	108.6	5.3	1.53
2	Q15459	splicing factor 3A subunit 1	88.9	5.2	1.61
3	P13797	T-plastin	70.9	5.5	1.59
4	P60709	actin cytoplasmic 1	42.1	5.3	1.50
5	P63104	14-3-3 zeta/delta	27.9	4.7	1.63
6	P52565	Rho GDP-dissociation inhibitor 1 (Rho GDI)	23.3	5.0	1.90
7	P30041	Peroxiredoxin-6 (PRDX6)	25.1	6.0	1.86

2. Investigations, results and discussion

In order to search for metastasis-related proteins, we analyzed differentially-expressed proteins between SW480 and SW620 by two-dimensional differential in-gel electrophoresis (2D-DIGE) (Fig. 1). As a result, 7 spots with at least a 1.5-fold-altered expression level were found by quantitative analysis, and these spots were identified by mass spectrometry (Table 1). Three molecules having a high SW620/SW480 expression ratio indicating a strong association with cancer metastasis were identified: Rho GDP-dissociation inhibitor alpha (Rho GDI), peroxiredoxin-6 (PRDX6) and 14-3-3 zeta/delta.

The expression profiles of these proteins were analyzed by immunohistochemistry using the TMA with colon cancer and multiple cancer tissues. Results of this analysis indicated that expression of PRDX6 and 14–3-3 zeta/delta had no relationship to the clinical status of cancer metastasis (data not shown). On the other hand, in positive cases of lymph node metastasis, the expression ratio of Rho GDI was significantly higher than in the negative cases. Furthermore, the same trend was seen when tissues from prostate cancer patients were analyzed (Table 2).

To confirm these results, the expression levels of Rho GDI protein in colon cancer cell lines with different metastatic potential (SW480 < SW620 < SW620-OK1 < SW620-OK2: Characteristics of SW620-OK1 and SW620-OK2 are described in *Experimental*) were investigated by western blot analysis (Fig. 2). The expression of Rho GDI was found to be up-regulated with the development of metastatic characteristics. These results suggested that Rho GDI is correlated with cancer metastasis.

Rho GDI has been identified as key regulator of Rho family GTPases. Activation of growth factor receptors and integrins can promote the exchange of GDP for GTP on Rho proteins (Bishop et al. 2000). Furthermore, GTP-bound Rho proteins interact with a range of effector molecules to modulate their activity or localization, and this leads to changes in cell behavior. It is clear that Rho family GTPases are involved in the control of cell morphology and motility (Etienne-Manneville et al. 2002; Hall et al. 1997; Van Aelst et al. 1997). The importance of Rho protein and Rho GDI in cancer progression, particularly in the area of metastasis, is becoming increasingly evident. Recently, some reports have indicated that the expression of Rho GDI was correlated with colorectal and breast cancer metastasis (Zhao et al. 2008; Kang et al. 2010). Thus, our findings are consistent with these reports and further suggest that the expression of Rho GDI is also correlated with prostate cancer metastasis. Consequently, Rho GDI should be considered as a diagnostic marker or new therapeutic target for cancer metastasis.

3. Experimental

3.1. Cell lines

SW480 is a human colorectal cancer cell line derived from a primary focus and SW620 is derived from a metastatic focus of the same patient. These cells were purchased from American Type Culture Collection and maintained at 37 °C using Leibovitz's L-15 medium (Wako) supplemented with 10% FCS. SW620-OK1 and -OK2 were established by the following procedure: 1×10^6 SW620 cells were injected into the spleens of nu/nu mice. After 8 weeks, SW620-OK1 was established from a liver metastatic focus. Furthermore, SW620-OK2 was established from SW620-OK1 using the same procedures.

3.2. 2D-DIGE analysis

Cell lysates were prepared from SW480 and SW620 and then solubilized with 7 M urea, 2 M thiourea, 4% CHAPS and 10 mM Tris-HCl (pH 8.5). The lysates were labeled at the ratio of 50 μg proteins: 400 pmol Cy3 or Cy5 protein-labeling dye (GE Healthcare Biosciences) in dimethylformamide according to the manufacturer's protocol. Briefly, the labelled samples were mixed with rehydration buffer (7 M urea, 2 M thiourea, 4% CHAPS, 2% DTT, 2% Pharmalyte (GE Healthcare Biosciences)) and applied to a 24-cm immobilized pH gradient gel strip (IPG-strip pH 4–7 NL) for separation in the first dimension. Samples for the spot-picking gel were prepared without labelling by Cy-dyes. For the second dimension separation, the IPG-strips were applied to SDS-PAGE gels (10% polyacrylamide and 2.7% N,N'-diallyltartardiamide gels). After electrophoresis, the gels were scanned with a laser fluoroimager (Typhoon Trio, GE Healthcare Biosciences). The spot-picking gel was scanned after staining with Deep Purple Total Protein Stain (GE Healthcare Biosciences). Quantitative analysis of protein spots was carried out with Decyder-DIA software (GE Healthcare Biosciences). For the antigen spots of interest, spots of 1 mm × 1 mm in size were picked using Ettan Spot Picker (GE Healthcare Biosciences).

3.3. In-gel tryptic digestion

Picked gel pieces were digested with trypsin as described below. The gel pieces were destained with 50% acetonitrile/50 mM NH_4HCO_3 for 20 min twice, dehydrated with 75% acetonitrile for 20 min, and then dried using a centrifugal concentrator. Next, 5 μl of 20 μl/ml trypsin (Promega) solution was added to each gel piece and incubated for 16 h at 37 °C. Three solutions were used to extract the resulting peptide mixtures from the gel pieces. First, 50 μl of 50% (v/v) acetonitrile in 0.1% (v/v) formic acid (FA) was added to the gel pieces, which were then sonicated for 5 min. Next, we collected the solution and added 80% (v/v) acetonitrile in 0.1% FA. Finally, 100% acetonitrile was added for the last extraction. The peptides were dried and then re-suspended in 10 μl of 0.1% FA.

3.4. Mass spectrometry and database search

Extracted peptides were analyzed by liquid chromatography Ultra High Resolution time-of-flight mass spectrometry (LC-UHR TOF/MS; maXis, Bruker Daltonics). The Mascot search engine (http://www.matrixscience.com) was initially used to query the entire theoretical tryptic peptide database as well as SwissProt (http://www.expasy.org/, a public domain database pro-

Table 2: Expression profile of Rho GDI in primary cancers with or without lymph node metastasis

	Number of Rho GDI positive cases (positive ratio)	
	in metastasis negative cases	in metastasis positive cases
Colon cancer*	11/14 (79%)	19/19 (100%)
Prostate cancer*	18/23 (78%)	11/11 (100%)

* $p < 0.05$: Mann Whitney U test

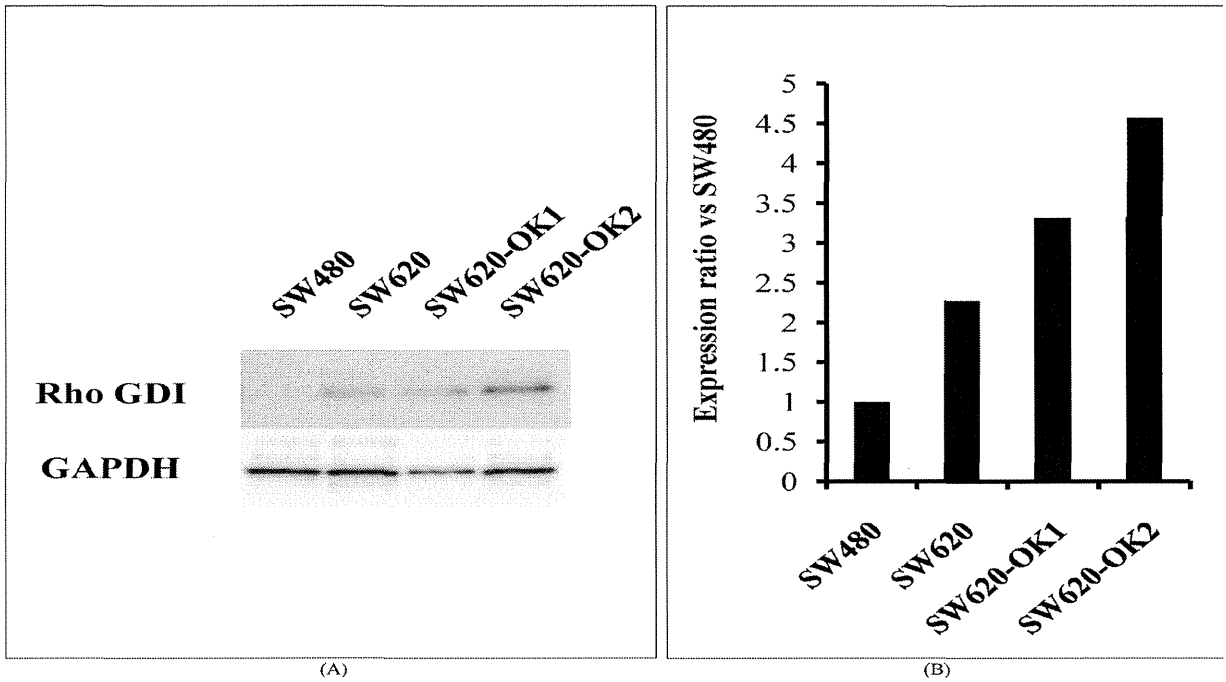

Fig. 2: Rho GDI expression levels in colon cancer cell lines with different metastatic abilities. Rho GDI expression levels in colon cancer cell lines (SW480, SW620, SW620-OK1, SW620-OK2) analyzed by western blotting (A). SW620-OK1, SW620-OK2 have been established as high metastatic sub-lines of SW620 using a mouse metastasis model. Intensity of the western blotting images was quantified by densitometry (B)

vided by the Swiss Institute of Bioinformatics). The search query assumed the following: (i) the peptides were monoisotopic (ii) methionine residues may be oxidized (iii) all cysteines are modified with iodoacetamide.

3.5. TMA Immunochemical staining

TMA slides with human colon cancer samples or multiple cancer samples (Biomax) were de-paraffinated in xylene and rehydrated in a graded series of ethanol washes. Heat-induced epitope retrieval was performed while maintaining the Target Retrieval Solution pH 9 (Dako) at the desired temperature according to manufacturer's instructions. After the treatment, endogenous peroxidase was blocked with 0.3% H_2O_2 in Tris-buffer saline (TBS) for 5 min. After washing twice with TBS, TMA slides were incubated with 10% BSA blocking solution for 30 min. The slides were then incubated with the anti-Rho GDI (Santa Cruz Biotechnology) for 60 min. After washing three times with wash buffer (Dako), each series of sections was incubated for 30 min with Envision + Dual Link (Dako). The reaction products were rinsed twice with wash buffer and then developed in liquid 3, 3'-diaminobenzidine (Dako) for 3 min. After the development, sections were counterstained with Mayer's hematoxylin. All procedures were performed using AutoStainer (Dako).

3.6. TMA Immunohistochemistry scoring

The optimized staining conditions for TMAs corresponding to human colon as well as multiple cancers were determined based on the co-existence of both positive and negative cells in the same tissue sample. Signals were considered positive when reaction products were localized in the expected cellular component. The criteria for scoring of stained tissues were as follows: the distribution score was 0 (0%), 1 (1–50%) or 2 (51–100%), indicating the percentage of positive cells among all tumor cells present in one tissue. The intensity of the signal (intensity score) was scored as 0 (no signal), 1 (weak), 2 (moderate) or 3 (marked). The distribution and intensity scores were then summed into a total score (TS) of TS0 (sum = 0), TS1 (sum = 2), TS2 (sum = 3), and TS3 (sum = 4–5). Throughout this study, TS0 or TS1 was regarded as negative, whereas TS2 or TS3 were regarded as positive.

3.7. Western Blot

Expression of Rho GDI in colon cancer cells was detected by anti-Rho GDI (Santa Cruz Biotechnology) and HRP conjugated anti-mouse IgG antibody (Sigma) using the ECL-plus system. Equal amounts of protein loading were confirmed by parallel β-actin immunoblotting, and signal quantification was performed by densitometric scanning.

Acknowledgements: This study was supported in part by Grants-in-Aid for Scientific Research from the Ministry of Education, Culture, Sports, Science and Technology of Japan, and from the Japan Society for the Promotion of Science (JSPS). This study was also supported in part by Health Labor Sciences Research Grants from the Ministry of Health, Labor and Welfare of Japan.

References

Bishop AL, Hall A (2000) Rho GTPases and their effector proteins. Biochem J 348: 241–255.

Davies RJ, Miller R, Coleman N (2005) Colorectal cancer screening: prospects for molecular stool analysis. Nat Rev Cancer 5: 199–209.

Etienne-Manneville S, Hall A (2002) Rho GTPases in cell biology. Nature 420: 629–635.

Hall A (1997). Rho GTPases and the Actin cytoskeleton. Science 279: 509–514.

Hanash S (2003) Disease proteomics. Nature 422: 226–232.

Imai S, Nagano K, Yoshida Y, Okamura T, Yamashita T, Abe Y, Yoshikawa T, Yoshioka Y, Kamada H, Mukai Y, Nakagawa S, Tsutsumi Y, Tsunoda S (2011). Development of an antibody proteomics system using a phage antibody library for efficient screening of biomarker proteins. Biomaterials 32: 162–169.

Kang S, Kim MJ, An H, Kim BG, Choi YP, Kang KS, Gao MQ, Park H, Na HJ, Kim HK, Yun HR, Kim DS, Cho NH (2010) Proteomic molecular portrait of interface zone in breast cancer. J Proteome Res 9: 5638–5645.

Liu R, Wang K, Yuan K, Wei Y, Huang C (2010) Integrative oncoproteomics strategies for anticancer drug discovery. Expert Rev Proteomics 7: 411–429.

Sahai E (2007). Illuminating the metastatic process. Nat Rev Cancer 7: 737–749.

Suehara Y, Tochigi N, Kubota D, Kikuta K, Nakayama R, Seki K, Yoshida A, Ichikawa H, Hasegawa T, Kaneko K, Chuman H, Beppu Y, Kawai A, Kondo T (2011) Secernin-1 as a novel prognostic biomarker candidate of synovial sarcoma revealed by proteomics. J Proteomics 74: 829–842.

Van Aelst L, D'Souza-Schorey C (1997) Rho GTPases and signaling networks. Genes Dev 11: 2295–2322.

Yoshida Y, Yamashita T, Nagano K, Imai S, Nabeshi H, Yoshikawa T, Yoshioka Y, Abe Y, Kamada H, Tsutsumi Y, Tsunoda S (2011) Limited expression of reticulocalbin-1 in lymphatic endothelial cells in lung tumor but not in normal lung. Biochem Biophys Res Commun 405: 610–614.

Zhao L, Wang H, Li J, Liu Y, Ding Y (2008) Overexpression of Rho GDP-dissociation inhibitor alpha is associated with tumor progression and poor prognosis of colorectal cancer. J Proteome Res 7: 3994–4003.

Higashisaka et al. Nanoscale Research Letters 2012, 7:555
http://www.nanoscalereslett.com/content/7/1/555

Nanoscale Research Letters
a SpringerOpen Journal

NANO EXPRESS Open Access

Hemopexin as biomarkers for analyzing the biological responses associated with exposure to silica nanoparticles

Kazuma Higashisaka[1†], Yasuo Yoshioka[1*†], Kohei Yamashita[1], Yuki Morishita[1], Huiyan Pan[1], Toshinobu Ogura[1], Takashi Nagano[1], Akiyoshi Kunieda[1], Kazuya Nagano[2], Yasuhiro Abe[3], Haruhiko Kamada[2,4], Shin-ichi Tsunoda[2,4], Hiromi Nabeshi[5], Tomoaki Yoshikawa[1] and Yasuo Tsutsumi[1,2,4*]

Abstract

Practical uses of nanomaterials are rapidly spreading to a wide variety of fields. However, potential harmful effects of nanomaterials are raising concerns about their safety. Therefore, it is important that a risk assessment system is developed so that the safety of nanomaterials can be evaluated or predicted. Here, we attempted to identify novel biomarkers of nanomaterial-induced health effects by a comprehensive screen of plasma proteins using two-dimensional differential in gel electrophoresis (2D-DIGE) analysis. Initially, we used 2D-DIGE to analyze changes in the level of plasma proteins in mice after intravenous injection via tail veins of 0.8 mg/mouse silica nanoparticles with diameters of 70 nm (nSP70) or saline as controls. By quantitative image analysis, protein spots representing >2.0-fold alteration in expression were found and identified by mass spectrometry. Among these proteins, we focused on hemopexin as a potential biomarker. The levels of hemopexin in the plasma increased as the silica particle size decreased. In addition, the production of hemopexin depended on the characteristics of the nanomaterials. These results suggested that hemopexin could be an additional biomarker for analyzing the biological responses associated with exposure to silica nanoparticles. We believe that this study will contribute to the development of biomarkers to ensure the safety of silica nanoparticles.

Keywords: Silica nanoparticle, Plasma proteins, Hemolysis, Biomarker

Background

Nanomaterials with particle sizes below 100 nm display unique properties compared to conventional materials with a submicron size. Various types of nanomaterials have been designed and produced for consumer and industrial applications such as medicine, cosmetics, and food [1,2]. As the use of nanomaterials increases, there is a growing need to ensure their safety because their unique properties might be associated with undesirable biological interactions [3,4]. However, current knowledge of the potential risk of nanomaterials is considered insufficient. Therefore, to facilitate the development of nanomaterials as a safe and usable product, it is important to develop guidelines for evaluation of their safety and efficacy.

Silica nanoparticles have been widely used in many consumer products such as cosmetics, food, and medicine because of their useful properties, including straightforward synthesis, relatively low cost, easy separation, and easy surface modification [5,6]. However, recent studies have found that silica nanoparticles induce substantial lung inflammation and are cytotoxic to various cell types [7,8]. Furthermore, our group showed that silica nanoparticles penetrate the skin and produce systemic exposure after topical application [9]. These findings underscore the need to examine biological effects after systemic exposure to silica nanoparticles. Our group also demonstrated that intravenous injection of silica nanoparticles with a diameter of 70 nm into mice

* Correspondence: yasuo@phs.osaka-u.ac.jp; ytsutsumi@phs.osaka-u.ac.jp
†Equal contributors
[1]Laboratory of Toxicology and Safety Science, Graduate School of Pharmaceutical Sciences, Osaka University, 1-6 Yamadaoka, Suita, Osaka 565-0871, Japan
[2]Laboratory of Biopharmaceutical Research, National Institute of Biomedical Innovation, 7-6-8, Saito-Asagi, Ibaraki, Osaka 567-0085, Japan
Full list of author information is available at the end of the article

might induce severe liver damage [9-12] and pregnancy complications such as resorption and fetal growth restriction [13]. We also showed that these pregnancy complications can be suppressed by amino or carboxyl group surface modification [11,13].

The development of safe nanomaterials requires not only an evaluation of safety, but also the ability to predict their biological effects. Molecular biomarkers constitute an objective indicator for correlating against various physiological conditions or variation of disease state [14,15]. Biomarker studies have the potential to provide valuable information to identify early biological events associated with the adverse health effects of engineered nanomaterials in a development stage more easily and rapidly [16]. Studies of biomarkers for nanomaterials have barely advanced, but it is envisaged that a biomarker profile for exposure to nanomaterials would represent the unity of local and systemic physiological responses induced as a result of exposure. Therefore, there is a need to identify and evaluate biomarkers for nanomaterials that would be suitable for predicting the potential toxicity of nanomaterials as well as to facilitate the development of nanomaterials that are safe. In this regard, our previous study used sodium dodecyl sulfate-polyacrylamide gel electrophoresis (SDS-PAGE) analysis to show that the acute-phase proteins, haptoglobin, C-reactive protein, and serum amyloid A (SAA), can act as useful biomarkers for analyzing the risk of exposure to nanomaterials and their associated toxicity [17]. However, SDS-PAGE analysis has limited capacity for a comprehensive screen for biomarkers because it is based only on differences in molecular weight of proteins. Proteomics-based analyses such as two-dimensional (2D) gel separation and mass spectrometry are more suitable approaches for such a comprehensive study. Here, we performed a screen for biomarkers of nanomaterials using two-dimensional differential in gel electrophoresis (2D-DIGE), which is a gel-based approach like SDS-PAGE but separates proteins on the basis of their molecular weight and isoelectric point. We used this approach to identify hemopexin as a potential biomarker for predicting the biological effects induced by silica nanoparticles.

Methods

Materials

Silica particles were purchased from Micromod Partikeltechnologie (Rostock/Warnemünde, Germany). Silica particles with diameters of 70, 300, and 1,000 nm (nSP70, nSP300, and mSP1000, respectively) and nSP70 with surface carboxyl and amino groups (nSP70-C and nSP70-N, respectively), were used in this study. The silica particles were suspended in saline, sonicated for 5 min, and vortexed for 1 min prior to use.

Animals

Female BALB/c mice were purchased from Nippon SLC, Inc. (Shizuoka, Japan) and were used at 6 to 8 weeks of age. The mice were housed in a ventilated animal room maintained at 20 ± 2°C with a 12-h light/12-h dark cycle. The mice had free access to water and forage (FR-2, Funabashi farm, Chiba, Japan). All of the animal experimental procedures used in this study were performed in accordance with the Osaka University and National Institute of Biomedical Innovation guidelines for the welfare of animals.

2D-DIGE analysis

The BALB/c mice were treated intravenously with 0.8 mg/mouse nSP70 or saline. After 24 h, blood samples were collected, and plasma was harvested by centrifuging blood at 13,800×*g* for 15 min. ProteoPrep (Sigma-Aldrich, Saint Louis, MO, USA) was used to remove albumin and immunoglobulin from the plasma according to the manufacturer's instructions. Plasma proteins were purified from the plasma of the nSP70- or saline-treated mice using a 2D-Clean up Kit (GE Healthcare Biosciences, Piscataway, NJ, USA) and were labeled at the ratio of 50 μg proteins:400 pmol Cy3 or Cy5 protein-labeling dye (GE Healthcare Biosciences) in dimethylformamide according to the manufacturer's protocol. Briefly, 50 μg of each labeled sample was mixed with rehydration buffer (7 M urea, 2 M thiourea, 4% 3-(3-cholamidepropyl) dimethylammonio-1-propanesulphonate, 2% dithiothreitol, 2% Pharmalyte; GE Healthcare Biosciences) and applied to a 24-cm immobilized pH gradient gel strip (immobilized pH gradient (IPG) strip pH 4 to 7 NL) for separation in the first dimension. Samples for the spot picking gel were prepared without labeling by Cy dyes. For the second-dimension separation, the IPG strips were applied to SDS-PAGE gels (10% polyacrylamide and 2.7% *N,N'*-diallyltartardiamide gels). After electrophoresis, the gels were scanned with a laser fluoroimager (Typhoon Trio, GE Healthcare Biosciences). The spot picking gel was scanned after staining with Deep Purple Total Protein Stain (GE Healthcare Biosciences). Quantitative analysis of protein spots was carried out with Decyder-DIA software (GE Healthcare Biosciences). Protein spots representing greater than twofold alteration in expression were picked using an Ettan Spot Picker (GE Healthcare Biosciences).

In-gel tryptic digestion

The gel pieces were destained with 50% acetonitrile (ACN)/25 mM NH_4HCO_3 for 10 min, dehydrated with 100% ACN for 10 min, and then dried using a centrifugal concentrator (TOMY SEIKO, Tokyo, Japan). Next, 8 μl of 20 μl/ml trypsin solution (Promega, Madison, WI, USA) diluted fivefold in 50 mM NH_4HCO_3 was

added to each gel piece, which was then incubated overnight at 37°C. We used three solutions to extract the resulting peptide mixtures from the gel pieces. First, 50 μl of 50% (*v*/*v*) ACN in 0.1% aqueous trifluoroacetic acid (TFA) was added to the gel pieces, which were then sonicated for 30 min. Next, we collected the solution and added 80% (*v*/*v*) ACN in 0.1% TFA. Finally, 100% ACN was added for the last extraction. The peptide solutions were dried and resuspended in 10 μl of 0.1% formic acid. The resulting peptide mixture was then analyzed by nano-flow liquid chromatography/tandem mass spectrometry (maXis, Bruker Daltonik GmbH, Bremen, Germany). The Mascot search engine (Matrix Science Inc., Boston, MA, USA) was initially used to query the entire theoretical tryptic peptide as well as the Swiss-Prot protein sequence database.

Measurement of hemopexin

The BALB/c mice were treated intravenously with 0.8 mg/mouse of the silica particles nSP70, nSP300, mSP1000, nSP70-C, and nSP70-N or with saline. Blood samples were collected at 2, 6, 24, 48, and 72 h after treatment. For assessment of the sensitivity of hemopexin levels to the concentration of silica particles, the BALB/c mice were treated intravenously with 0.05, 0.2, or 0.8 mg/mouse nSP70. After 24 h, blood samples were collected, and plasma was harvested by centrifuging blood at 13,800×*g* for 15 min. Plasma levels of hemopexin were measured using a commercial enzyme-linked immunosorbent assay (ELISA) kit (Life Diagnostics, West Chester, PA, USA), according to the manufacturer's instructions.

Plasma biochemistry

The BALB/c mice were treated intravenously with 0.8 mg/mouse nSP70 or saline. After 2, 6, 24, and 48 h, blood samples were collected, and plasma was harvested by centrifuging blood at 13,800×*g* for 15 min. Total hemoglobin and heme in the blood of the nSP70-treated mice were determined by BioAssay Systems QuantiChrom™ Assay Kits (BioAssay Systems, Hayward, CA, USA). Also, plasma levels of total bilirubin (TBIL) and direct bilirubin (DBIL) were measured by a biochemical auto analyzer, FUJI DRI-CHEM 7000 (Fujifilm, Tokyo, Japan), and the level of indirect bilirubin was calculated from these values.

Statistical analysis

All results are expressed as means ± standard error of the mean (SEM). Statistical comparisons between groups were performed by one-way analysis of variance (ANOVA) with the Bonferroni test.

Results

Characteristics of silica particles

Silica particles are well suited for studying the influence of nanomaterial size on biodistribution and various biological effects because they show much better dispersibility in aqueous solutions than most other nanomaterials [18]. We used three different-sized silica particles with diameters between 70 and 1,000 nm (nSP70, nSP300, and mSP1000) and nSP70 with carboxyl (nSP70-C) and amino (nSP70-N) surface functional groups. As we have described previously [9,10,13], all silica nanoparticles were confirmed by transmission electron microscopy to be smooth-surfaced spheres. The hydrodynamic diameters of nSP70, nSP300, and mSP1000 were 65, 322, and 1,140 nm, respectively, and their zeta potentials or overall surface potentials were −53, −62, and −67 mV, respectively. For nSP70-C and nSP70-N, the hydrodynamic diameters were 70 and 72 nm, respectively, and their zeta potentials were −76 and −29 mV, respectively. These results indicate that the carboxyl and amino surface modifications altered the surface charge of the particles. The size distribution spectrum of each set of silica particles showed a single peak, and the measured hydrodynamic diameter corresponded almost precisely to the primary particle size of each set of silica particles. These results indicate that the silica particles used in this study were well dispersed in solution.

2D-DIGE analysis and identification of differentially expressed proteins

To identify protein biomarkers of nanomaterials in mice, we analyzed changes in the levels of plasma proteins following treatment with nSP70 by using 2D-DIGE. Plasma proteins isolated after treatment with saline or 0.8 mg/mouse nSP70 were labeled with Cy3 and Cy5, respectively, and were used for 2D-DIGE analysis. The reason why we chose the dose of silica particles for treatment is that none of the silica particles induced any significant changes in the levels of aspartate aminotransferase (AST), alanine aminotransferase (ALT), and blood urea nitrogen and that all parameters remained within the physiological range, as we have previously reported [17]. Quantitative image analysis revealed 59 spots showing increased protein levels and 23 spots showing decreased protein levels in the plasma of nSP70-treated mice compared with controls. We selected a total of eight candidate spots showing the highest increases and decreases in protein expression levels. Then, liquid chromatography/time-of-flight/mass spectrometry (LC/TOF/MS) analysis of the spots subsequently identified seven different proteins (Figure 1). Among these proteins, haptoglobin, hemopexin, and alpha-1-acid glycoprotein 1, which are acute-phase proteins, displayed increased expression in the plasma of nSP70-treated mice. Four proteins, including inter-alpha-trypsin inhibitor, complement C4-B,

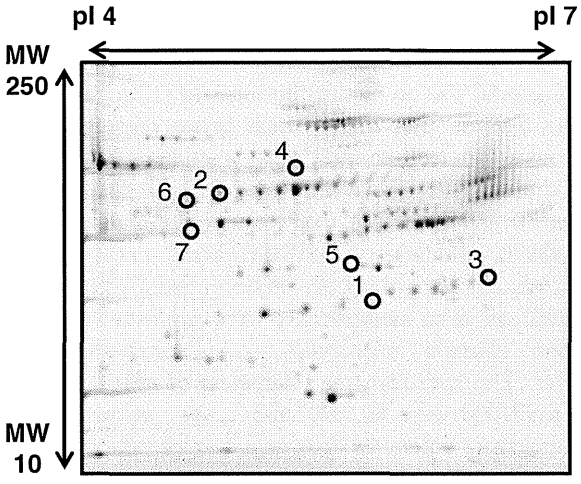

Figure 1 2D-DIGE image of fluorescent-labeled proteins. Proteins from the plasma after treatment with saline or nSP70 were labeled with Cy3 and Cy5, respectively, and used for performing 2D electrophoresis.

Cullin-4A, and serotransferrin, displayed decreased expression in the plasma of nSP70-treated mice (Table 1). These findings are consistent with the results of our previous study identifying haptoglobin, showing the highest level in this study, as a candidate biomarker using SDS-PAGE analysis. We selected a candidate biomarker from among the proteins which displayed increased expression at first. However, in the future, there is a need to identify various biomarkers by evaluating candidate proteins which displayed not only increased expression but also decreased expression to improve the accuracy for predicting the biological effects induced by nanomaterials. Here, we focused on hemopexin, which showed the second highest expression level among the identified candidate biomarkers after haptoglobin.

Plasma hemopexin levels after treatment with silica particles

Hemopexin is known as an acute-phase protein, mainly synthesized in the liver [19]. To assess the potential of hemopexin as a biomarker, we examined whether there were time-dependent changes in the plasma levels of hemopexin levels after treatment with different-sized silica particles. The BALB/c mice were treated intravenously with 0.8 mg/mouse nSP70, nSP300, or mSP1000. After 6, 24, or 72 h, we examined the plasma levels of hemopexin by ELISA. We observed no changes in the plasma levels of hemopexin in mice treated with nSP300 or mSP1000 over the time course of the experiment. However, mice treated with nSP70 showed an increase in plasma levels of hemopexin at 24 h after treatment, and the plasma level of hemopexin in nSP70-treated mice remained significantly higher than that of controls at 72 h after treatment (Figure 2A). These results indicate that the smaller the particle size, the greater the increase in plasma levels of hemopexin induced by silica particles. We then assessed the sensitivity of hemopexin induction to lower concentrations of silica particles. The BALB/c mice were treated intravenously with 0.05, 0.2, or 0.8 mg/mouse nSP70. After 24 h, we examined the plasma levels of hemopexin by ELISA and found that the plasma level of hemopexin increased in a dose-dependent manner (Figure 2B). These results indicate that the level of induction of hemopexin is dependent on the concentration of silica particles. Taken together, these findings highlight the potential of hemopexin as a valuable biomarker for analyzing the risk and toxicity of exposure to silica nanoparticles. Now, to evaluate the sensitivity of hemopexin to serve as a biomarker of a more realistic exposure, we have assessed the response of hemopexin to silica nanoparticles introduced via different routes.

Hemolytic activity of silica nanoparticles

Hemopexin is a heme-binding plasma glycoprotein that forms the second line of defense against hemoglobin-mediated oxidative damage during intravascular hemolysis [20]. Intravascular hemolysis causes the release of massive amounts of hemoglobin and heme into the plasma, where they are rapidly bound by haptoglobin and hemopexin, respectively [21]. Because nSP70 induced an increase in the plasma levels of haptoglobin and hemopexin in mice, we investigated the possibility

Table 1 Identification of candidate proteins as biomarkers

Spot	Protein name	Accession number	MW (kD)	pI	Expression ratio (nSP70/saline) (fold)
1	Haptoglobin	[Swiss-Prot:Q61646]	38.75	5.88	375.44
2	Hemopexin	[Swiss-Prot:Q91X72]	51.34	7.92	3.25
3	Alpha-1-acid glycoprotein 1	[Swiss-Prot:Q60590]	23.89	5.58	3.05
4	Inter-alpha-trypsin inhibitor	[Swiss-Prot:Q61703]	105.93	6.82	0.40
5	Complement C4-B	[Swiss-Prot:P01029]	192.89	7.38	0.39
6	Cullin-4A	[Swiss-Prot:Q3TCH7]	87.75	8.53	0.37
7	Serotransferrin	[Swiss-Prot:Q921I1]	76.72	6.94	0.30

The differentially expressed spots were identified by LC/TOF/MS. pI, isoelectric point.

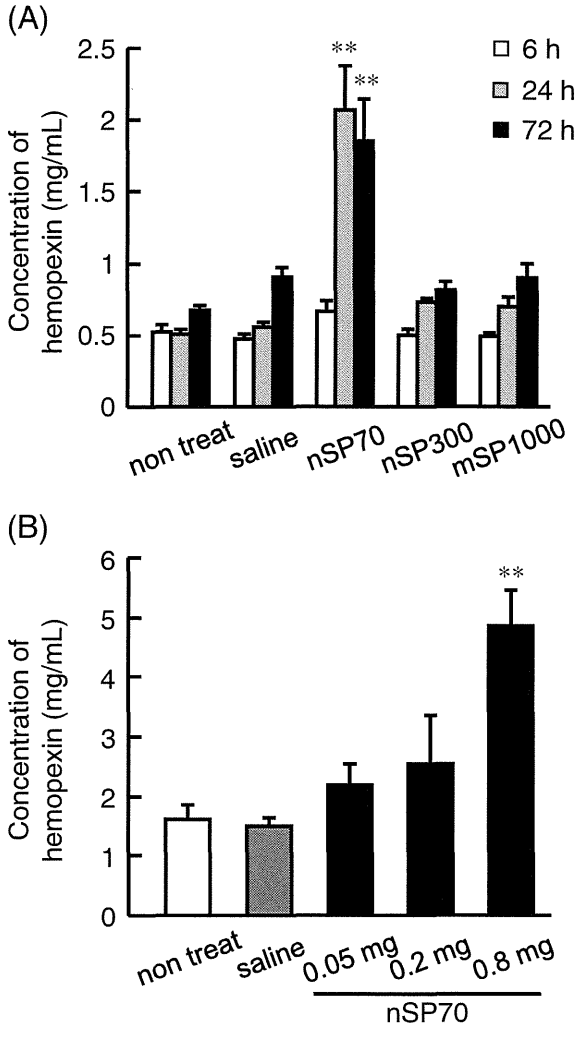

Figure 2 Plasma levels of hemopexin after treatment with silica particles. BALB/c mice were treated intravenously with 0.8 mg/mouse nSP70, nSP300, or mSP1000. (**A**) After 6, 24, and 72 h, the plasma levels of hemopexin in the mice were determined by ELISA. (**B**) BALB/c mice were treated intravenously with 0.05, 0.2, or 0.8 mg/mouse nSP70. After 24 h, blood samples were collected. The plasma levels of hemopexin in treated mice were determined by ELISA. Data are presented as mean ± SEM ($n = 5$; Double asterisks denote $P < 0.01$ versus the value for saline-treated group by ANOVA).

that silica nanoparticles could induce hemolytic activity. We assessed plasma levels of heme and hemoglobin 2, 6, 24, or 48 h after treatment of the BALB/c mice intravenously with 0.8 mg/mouse of nSP70. At this dose, nSP70 did not induce any significant increases in the plasma levels of heme (Figure 3A) or hemoglobin (Figure 3B) at all time points.

During hemolysis, hemoglobin is released into the plasma from damaged red blood cells and leads to an increase in plasma levels of indirect bilirubin [22-24]. Thus, although nSP70 did not induce a significant increase in the plasma levels of heme or hemoglobin, we investigated whether nSP70 induced hemolytic activity that resulted in an increased plasma level of indirect bilirubin. Following treatment of mice with nSP70, we measured plasma levels of TBIL and DBIL and calculated the level of indirect bilirubin from these values. We found no changes in the plasma levels of TBIL (Figure 3C), DBIL (Figure 3D), or indirect bilirubin (Figure 3E) over the time course of the experiment. Taken together, these results clearly show that nSP70 does not induce hemolytic activity in mice under these conditions.

Surface modification of nSP70

Previously, we demonstrated that surface properties of silica nanoparticles play an important role in determining their safety [11,13]. For instance, our group showed that surface modification of nSP70 with amine or carboxyl groups altered the intracellular distribution of the nanoparticles, had an effect on cell proliferation [11], and suppressed toxic biological effects of silica particles such as inflammatory responses. To assess whether hemopexin could predict the strength of toxicity induced by silica nanoparticles, we examined the plasma levels of hemopexin in the mice after administration of nSP70 with amino or carboxyl group surface modifications. The BALB/c mice were treated intravenously with 0.8 mg/mouse of nSP70, nSP70-C, or nSP70-N. After 2, 6, 24, or 48 h, we examined the plasma levels of hemopexin by ELISA. The mice treated with nSP70, nSP70-C, and nSP70-N did not show any elevated level of hemopexin at 2 or 6 h. At 24 h, the plasma level of hemopexin in mice treated with nSP70-N was significantly lower than that in mice treated with unmodified nSP70. On the other hand, the plasma level of hemopexin in mice treated with nSP70-C was similar to that in nSP70-treated mice and significantly higher than that in saline-treated mice (Figure 4A). At the same time, the plasma levels of haptoglobin (Figure 4B) and SAA (Figure 4C) in mice treated with nSP70-C were significantly lower than those in nSP70-treated mice, which is consistent with our previously reported results [17]. These results indicate that there are differences in the mechanisms underlying the production of hemopexin and other acute-phase proteins induced by nSP70-C.

Discussion

By using biomarkers, we are able to predict not only the present disease and clinical condition, but also the risk of acquiring disease in the future. Therefore, it is necessary to progress studies of biomarkers for nanomaterials because very little information is available on the biological effects of nanomaterials. Here, we used 2D-DIGE analysis to perform a comprehensive screen of plasma

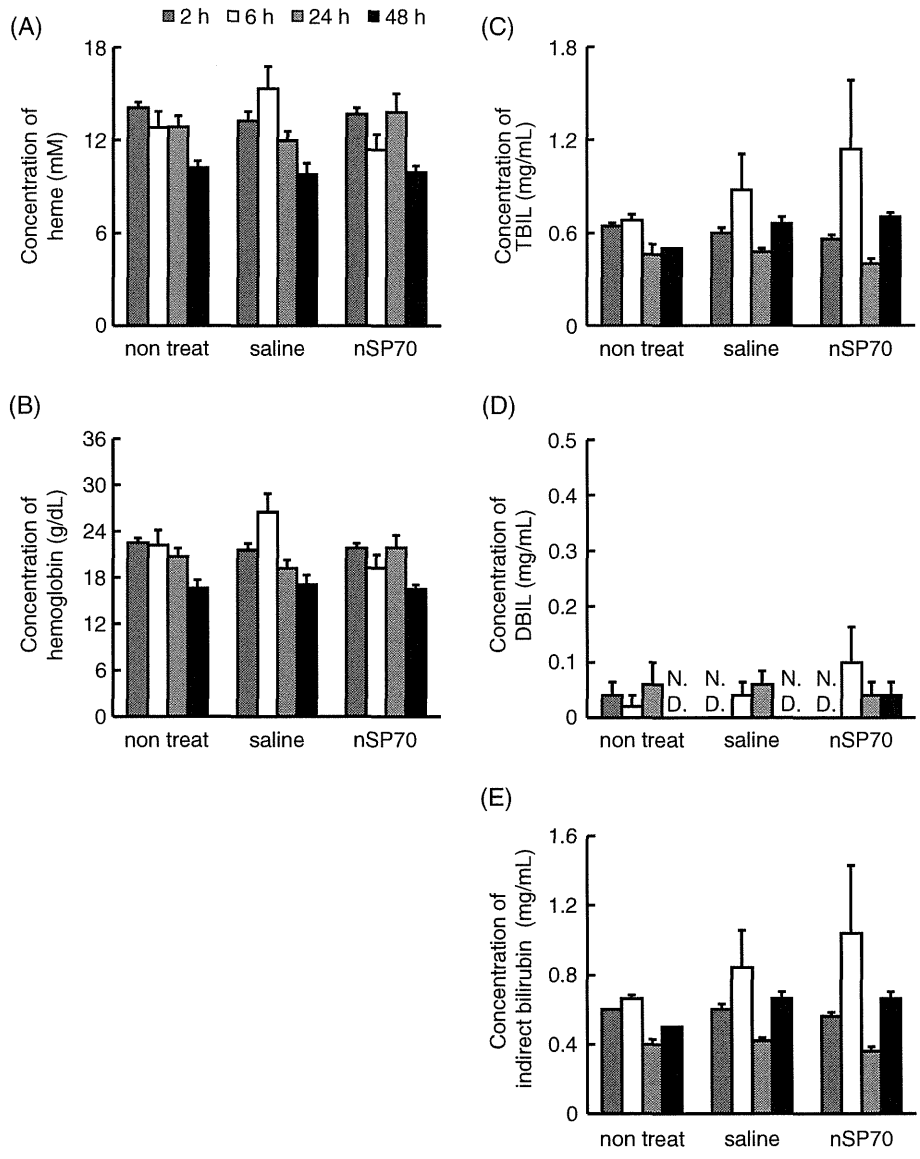

Figure 3 Hemolytic activity of silica nanoparticles. BALB/c mice were treated intravenously with 0.8 mg/mouse nSP70. After 2, 6, 24, and 48 h, we examined the level of (**A**) total heme and (**B**) hemoglobin in the blood of treated mice. The levels of (**C**) TBIL and (**D**) DBIL were measured, and (**E**) the level of indirect bilirubin was calculated from these values.

proteins to identify protein biomarkers of nanomaterials. We identified hemopexin (Table 1) as a useful biomarker for analyzing the biological responses associated with exposure to silica nanoparticles. Because 2D-DIGE is a proteomic method, this approach has potential to uncover the as yet unknown biological effects of nanomaterials.

On the other hand, an inherent disadvantage of 2D electrophoresis is the poor resolution of hydrophobic proteins [25,26]. Hence, it is likely that integral membrane proteins are strongly underrepresented. Isobaric tags for relative and absolute quantification or iTRAQ is a comprehensive gel-free quantitative proteomic method based on mass spectrometry [27,28]. This approach can be used to generate proteomic profiles that reflect the pathological state of organs and aid in the early detection of diseases [29,30]. We envisage that a combination of comprehensive proteomic methods would help to identify potential toxicities of nanomaterials during their development and contribute to the establishment of strategies to ensure their safety.

Silica materials with amorphous particle morphology are known to cause the hemolysis of mammalian red blood cells [31,32]. For this reason, we investigated the possibility that silica nanoparticles could induce hemolytic activity. While the exact mechanism is still

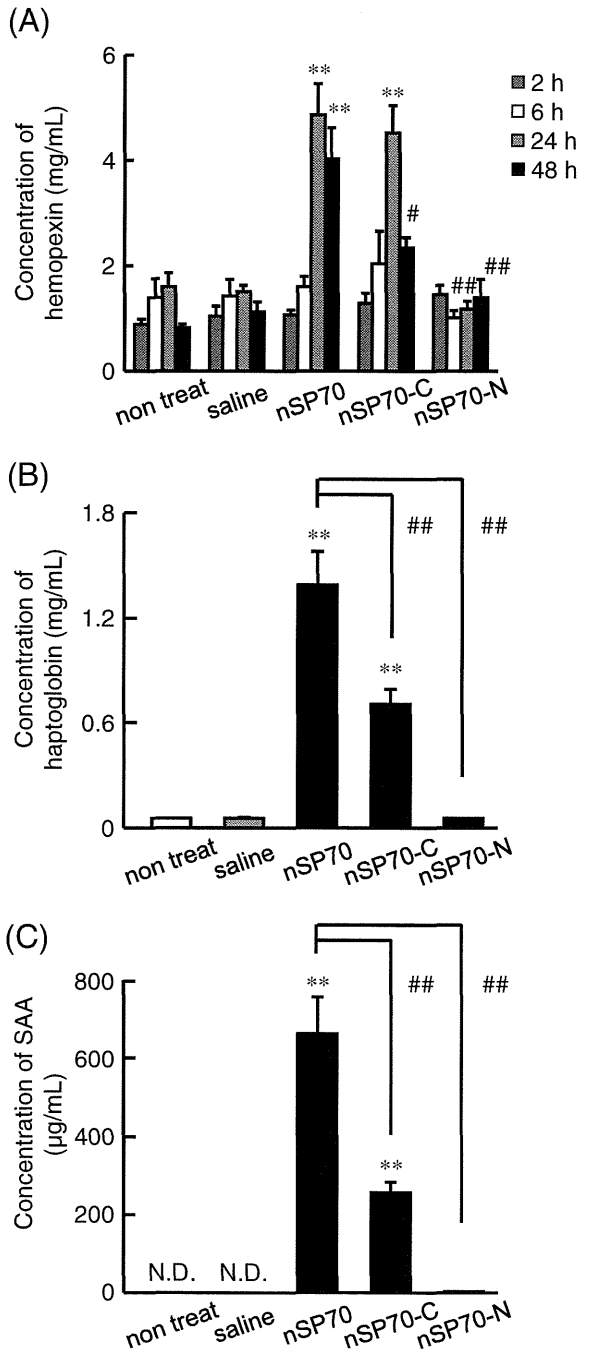

Figure 4 Responses of hemopexin by the exposure to surface modified nSP70. BALB/c mice were treated intravenously with nSP70 modified with amino (nSP70-N) or carboxyl (nSP70-C) groups at 0.8 mg/mouse. (**A**) After 2, 6, 24, and 48 h, the levels of hemopexin in the plasma of treated mice were examined by ELISA. The plasma levels of (**B**) haptoglobin and (**C**) SAA were determined by ELISA after 24 h. Data are presented as mean ± SEM. ($n = 5$; Double asterisks denote $P < 0.01$ versus the value for the saline-treated group by ANOVA, single hash denotes $P < 0.05$, and double hash denote $P < 0.01$ versus the value for the nSP70-treated group by ANOVA).

under investigation, most reports agree that the hemolytic activity of silica particles is related to surface characteristics such as area and curvature [33-35]. However, we found that nSP70 at 0.8 mg/mouse does not induce hemolytic activity through elevation of haptoglobin and hemopexin (Figure 3). We are continuing investigations to understand the biological mechanisms associated with the elevation of hemopexin after exposure to silica nanoparticles.

We then examined the effects of surface modification of silica nanoparticles on the production of hemopexin. Compared to controls, hemopexin was not induced by nSP70-N but was induced to a significantly higher level by nSP70-C, which was a similar level to that induced by unmodified nSP70 (Figure 4A). On the other hand, the plasma levels of haptoglobin (Figure 4B) and SAA (Figure 4C) in mice treated with nSP70-C were significantly lower than those in mice treated with nSP70, as reported previously [17]. These results suggest that the production of acute-phase proteins depends on the characteristics of the nanomaterials and that nSP70-C induces some biological effects associated with the elevation of hemopexin. Increased hemopexin levels have been found in patients with diabetes mellitus and are associated with some malignancies, such as malignant melanoma and breast cancer [20,36,37]. Elevated hemopexin levels have also been found in inflammatory psychiatric disorders, such as major depression, schizophrenia, and mania [38]. Taken together, these findings suggest that hemopexin might be associated with these diseases so it is possible that the induced elevation of hemopexin by both nSP70 and nSP70-C is related to the induction of inflammatory responses. Therefore, we are currently analyzing not only the mechanisms underlying the differences in production of hemopexin, haptoglobin, and SAA induced by nSP70-C and nSP70, but also the relationship. It could be speculated that there are differences between the fates of the injected nSP70 and nSP70-C. Therefore, there is a need to evaluate the distribution or accumulation of the injected nanoparticles in the liver where acute-phase proteins are known to be produced. An understanding of these mechanisms will advance the use of biomarkers for different purposes and improve the predictive value of these biomarkers.

Hemopexin is one of the acute-phase proteins released from the liver, and its production is known to be regulated by cytokines. For instance, interleukin (IL)-6 and IL-22 induce the hepatic production of circulating SAA [39,40]. Furthermore, it is conceivable that instead of inflammatory cytokines, small silica particles act directly on the liver to induce the release of acute-phase proteins. However, nSP70, at this dose, did not induce any significant elevation of liver injury or dysfunction

markers, such as ALT or AST. Therefore, it is unclear why nanomaterials induce the production of acute-phase proteins. We are currently analyzing the detailed mechanism by which silica particles induce acute-phase proteins.

Conclusions

We demonstrated that 2D-DIGE analysis is a useful approach for identifying novel biomarkers of nanomaterials. Using this approach, we identified hemopexin as a useful biomarker and showed here that hemopexin can act as a useful biomarker for analyzing the biological responses associated with exposure to silica nanoparticles. We believe that this study will contribute to the development of biomarkers for ensuring the safety of silica nanoparticles.

Abbreviations

2D: Two-dimensional; 2D-DIGE: Two-dimensional differential in gel electrophoresis; ACN: Acetonitrile; ALT: Alanine amino transferase; AST: Aspartate amino transferase; DBIL: Direct bilirubin; ELISA: Enzyme-linked immunosorbent assay; IL: Interleukin; IPG: Immobilized pH gradient; iTRAQ: Isobaric tags for relative and absolute quantification; LC/TOF/MS: Liquid chromatography/time-of-flight/mass spectrometry; SAA: Serum amyloid A; SDS-PAGE: Sodium dodecyl sulfate-polyacrylamide gel electrophoresis; TBIL: Total bilirubin; TFA: Trifluoroacetic acid.

Competing interests

The authors declare that they have no competing interests.

Authors' contributions

KH and YY designed the study. KH, KY, YM, HP, TO, TN, and AK performed the experiments. KH and YY collected and analyzed the data. KH and YY wrote the manuscript. KN, YA, HK, ST, HN, and TY gave technical support and conceptual advice. YT supervised all of the projects. All authors discussed the results and commented on the manuscript. All authors read and approved the final manuscript.

Acknowledgments

This study was supported in part by Grants-in-Aid for Scientific Research from the Ministry of Education, Culture, Sports, Science and Technology of Japan and from the Japan Society for the Promotion of Science (JSPS). This study was also supported in part by the following: Health Labour Sciences Research Grants from the Ministry of Health, Labor and Welfare of Japan; Health Sciences Research Grants for Research on Publicly Essential Drugs and Medical Devices from the Japan Health Sciences Foundation; the Global Environment Research Fund from the Minister of the Environment; the Knowledge Cluster Initiative; The Nagai Foundation Tokyo; the Cosmetology Research Foundation; the Smoking Research Foundation; the Research Foundation for Pharmaceutical Sciences; and The Japan Food Chemical Research Foundation.

Author details

[1]Laboratory of Toxicology and Safety Science, Graduate School of Pharmaceutical Sciences, Osaka University, 1-6 Yamadaoka, Suita, Osaka 565-0871, Japan. [2]Laboratory of Biopharmaceutical Research, National Institute of Biomedical Innovation, 7-6-8, Saito-Asagi, Ibaraki, Osaka 567-0085, Japan. [3]Cancer Biology Research Center, Sanford Research/USD, 2301 E. 60th Street N, Sioux Falls, SD 57104, USA. [4]The Center for Advanced Medical Engineering and Informatics, Osaka University, 1-6, Yamadaoka, Suita, Osaka 565-0871, Japan. [5]Division of Foods, National Institute of Health Sciences, 1-18-1 Kamiyoga, Setagaya-ku, Tokyo 158-8501, Japan.

Received: 16 July 2012 Accepted: 21 September 2012
Published: 8 October 2012

References

1. Augustin MA, Sanguansri P: **Nanostructured materials in the food industry.** *Adv Food Nutr Res* 2009, **58**:183–213.
2. Bowman DM, van Calster G, Friedrichs S: **Nanomaterials and regulation of cosmetics.** *Nat Nanotechnol* 2010, **5**:92.
3. Kagan VE, Bayir H, Shvedova AA: **Nanomedicine and nanotoxicology: two sides of the same coin.** *Nanomedicine* 2005, **1**:313–316.
4. Nel A, Xia T, Madler L, Li N: **Toxic potential of materials at the nanolevel.** *Science* 2006, **311**:622–627.
5. Merget R, Bauer T, Kupper HU, Philippou S, Bauer HD, Breitstadt R, Bruening T: **Health hazards due to the inhalation of amorphous silica.** *Arch Toxicol* 2002, **75**:625–634.
6. Knopp D, Tang D, Niessner R: **Review: bioanalytical applications of biomolecule-functionalized nanometer-sized doped silica particles.** *Anal Chim Acta* 2009, **647**:14–30.
7. Napierska D, Thomassen LC, Lison D, Martens JA, Hoet PH: **The nanosilica hazard: another variable entity.** *Part Fibre Toxicol* 2010, **7**:39.
8. Lankoff A, Arabski M, Wegierek-Ciuk A, Kruszewski M, Lisowska H, Banasik-Nowak A, Rozga-Wijas K, Wojewodzka M, Słomkowski S: **Effect of surface modification of silica nanoparticles on toxicity and cellular uptake by human peripheral blood lymphocytes in vitro.** *Nanotoxicology* 2012. doi:10.3109/17435390.2011.649796.
9. Nabeshi H, Yoshikawa T, Matsuyama K, Nakazato Y, Matsuo K, Arimori A, Isobe M, Tochigi S, Kondoh S, Hirai T, Akase T, Yamashita T, Yamashita K, Yoshida T, Nagano K, Abe Y, Yoshioka Y, Kamada H, Imazawa T, Itoh N, Nakagawa S, Mayumi T, Tsunoda S, Tsutsumi Y: **Systemic distribution, nuclear entry and cytotoxicity of amorphous nanosilica following topical application.** *Biomaterials* 2011, **32**:2713–2724.
10. Nabeshi H, Yoshikawa T, Matsuyama K, Nakazato Y, Tochigi S, Kondoh S, Hirai T, Akase T, Nagano K, Abe Y, Yoshioka Y, Kamada H, Itoh N, Tsunoda S, Tsutsumi Y: **Amorphous nanosilica induce endocytosis-dependent ROS generation and DNA damage in human keratinocytes.** *Part Fibre Toxicol* 2011, **8**:1.
11. Nabeshi H, Yoshikawa T, Arimori A, Yoshida T, Tochigi S, Hirai T, Akase T, Nagano K, Abe Y, Kamada H, Tsunoda S, Itoh N, Yoshioka Y, Tsutsumi Y: **Effect of surface properties of silica nanoparticles on their cytotoxicity and cellular distribution in murine macrophages.** *Nanoscale Res Lett* 2011, **6**:93.
12. Nabeshi H, Yoshikawa T, Matsuyama K, Nakazato Y, Arimori A, Isobe M, Tochigi S, Kondoh S, Hirai T, Akase T, Yamashita T, Yamashita K, Yoshida T, Nagano K, Abe Y, Yoshioka Y, Kamada H, Imazawa T, Itoh N, Kondoh M, Yagi K, Mayumi T, Tsunoda S, Tsutsumi Y: **Amorphous nanosilicas induce consumptive coagulopathy after systemic exposure.** *Nanotechnology* 2012, **23**:045101.
13. Yamashita K, Yoshioka Y, Higashisaka K, Mimura K, Morishita Y, Nozaki M, Yoshida T, Ogura T, Nabeshi H, Nagano K, Abe Y, Kamada H, Monobe Y, Imazawa T, Aoshima H, Shishido K, Kawai Y, Mayumi T, Tsunoda S, Itoh N, Yoshikawa T, Yanagihara I, Saito S, Tsutsumi Y: **Silica and titanium dioxide nanoparticles cause pregnancy complications in mice.** *Nat Nanotechnol* 2011, **6**:321–328.
14. Casado B, Iadarola P, Luisetti M, Kussmann M: **Proteomics-based diagnosis of chronic obstructive pulmonary disease: the hunt for new markers.** *Expert Rev Proteomics* 2008, **5**:693–704.
15. Ferte C, Andre F, Soria JC: **Molecular circuits of solid tumors: prognostic and predictive tools for bedside use.** *Nat Rev Clin Oncol* 2010, **7**:367–380.
16. Li N, Nel AE: **Feasibility of biomarker studies for engineered nanoparticles: what can be learned from air pollution research.** *J Occup Environ Med* 2011, **53**:S74–79.
17. Higashisaka K, Yoshioka Y, Yamashita K, Morishita Y, Fujimura M, Nabeshi H, Nagano K, Abe Y, Kamada H, Tsunoda S, Yoshikawa T, Itoh N, Tsutsumi Y: **Acute phase proteins as biomarkers for predicting the exposure and toxicity of nanomaterials.** *Biomaterials* 2011, **32**:3–9.
18. He X, Nie H, Wang K, Tan W, Wu X, Zhang P: **In vivo study of biodistribution and urinary excretion of surface-modified silica nanoparticles.** *Anal Chem* 2008, **80**:9597–9603.
19. Tolosano E, Altruda F: **Hemopexin: structure, function, and regulation.** *DNA Cell Biol* 2002, **21**:297–306.
20. Delanghe JR, Langlois MR: **Hemopexin: a review of biological aspects and the role in laboratory medicine.** *Clin Chim Acta* 2001, **312**:13–23.

21. Vinchi F, Gastaldi S, Silengo L, Altruda F, Tolosano E: **Hemopexin prevents endothelial damage and liver congestion in a mouse model of heme overload.** *Am J Pathol* 2008, **173**:289–299.
22. Lagan AL, Melley DD, Evans TW, Quinlan GJ: **Pathogenesis of the systemic inflammatory syndrome and acute lung injury: role of iron mobilization and decompartmentalization.** *Am J Physiol Lung Cell Mol Physiol* 2008, **294**:L161–174.
23. Nielsen MJ, Moestrup SK: **Receptor targeting of hemoglobin mediated by the haptoglobins: roles beyond heme scavenging.** *Blood* 2009, **114**:764–771.
24. Nielsen MJ, Moller HJ, Moestrup SK: **Hemoglobin and heme scavenger receptors.** *Antioxid Redox Signal* 2010, **12**:261–273.
25. Lopez JL: **Two-dimensional electrophoresis in proteome expression analysis.** *J Chromatogr B Analyt Technol Biomed Life Sci* 2007, **849**:190–202.
26. Sa-Correia I, Teixeira MC: **2D electrophoresis-based expression proteomics: a microbiologist's perspective.** *Expert Rev Proteomics* 2010, **7**:943–953.
27. Aggarwal K, Choe LH, Lee KH: **Shotgun proteomics using the iTRAQ isobaric tags.** *Brief Funct Genomic Proteomic* 2006, **5**:112–120.
28. Treumann A, Thiede B: **Isobaric protein and peptide quantification: perspectives and issues.** *Expert Rev Proteomics* 2010, **7**:647–653.
29. Xu J, Khor KA, Sui J, Zhang J, Tan TL, Chen WN: **Comparative proteomics profile of osteoblasts cultured on dissimilar hydroxyapatite biomaterials: an iTRAQ-coupled 2-D LC-MS/MS analysis.** *Proteomics* 2008, **8**:4249–4258.
30. Yang X, Yang S, Wang J, Zhang X, Wang C, Hong G: **Expressive proteomics profile changes of injured human brain cortex due to acute brain trauma.** *Brain Inj* 2009, **23**:830–840.
31. Gerashchenko BI, Gun'ko VM, Gerashchenko II, Mironyuk IF, Leboda R, Hosoya H: **Probing the silica surfaces by red blood cells.** *Cytometry* 2002, **49**:56–61.
32. Murashov V, Harper M, Demchuk E: **Impact of silanol surface density on the toxicity of silica aerosols measured by erythrocyte haemolysis.** *J Occup Environ Hyg* 2006, **3**:718–723.
33. Slowing II, Wu CW, Vivero-Escoto JL, Lin VS: **Mesoporous silica nanoparticles for reducing hemolytic activity towards mammalian red blood cells.** *Small* 2009, **5**:57–62.
34. Lin YS, Haynes CL: **Impacts of mesoporous silica nanoparticle size, pore ordering, and pore integrity on hemolytic activity.** *J Am Chem Soc* 2010, **132**:4834–4842.
35. Yu T, Malugin A, Ghandehari H: **Impact of silica nanoparticle design on cellular toxicity and hemolytic activity.** *ACS Nano* 2011, **5**:5717–5728.
36. Manuel Y, Defontaine MC, Bourgoin JJ, Dargent M, Sonneck JM: **Serum haemopexin levels in patients with malignant melanoma.** *Clin Chim Acta* 1971, **31**:485–486.
37. Coombes RC, Powles TJ, Neville AM: **Evaluation of biochemical markers in breast cancer.** *Proc R Soc Med* 1977, **70**:843–845.
38. Maes M, Delange J, Ranjan R, Meltzer HY, Desnyder R, Cooremans W, Scharpe S: **Acute phase proteins in schizophrenia, mania and major depression: modulation by psychotropic drugs.** *Psychiatry Res* 1997, **66**:1–11.
39. Immenschuh S, Song DX, Satoh H, Muller-Eberhard U: **The type II hemopexin interleukin-6 response element predominates the transcriptional regulation of the hemopexin acute phase responsiveness.** *Biochem Biophys Res Commun* 1995, **207**:202–208.
40. Liang SC, Nickerson-Nutter C, Pittman DD, Carrier Y, Goodwin DG, Shields KM, Lambert AJ, Schelling SH, Medley QG, Ma HL, Collins M, Dunussi-Joannopoulos K, Fouser LA: **IL-22 induces an acute-phase response.** *J Immunol* 2010, **185**:5531–5538.

doi:10.1186/1556-276X-7-555
Cite this article as: Higashisaka *et al.*: Hemopexin as biomarkers for analyzing the biological responses associated with exposure to silica nanoparticles. *Nanoscale Research Letters* 2012 **7**:555.

nature medicine

A bispecific antibody to factors IXa and X restores factor VIII hemostatic activity in a hemophilia A model

Takehisa Kitazawa[1], Tomoyuki Igawa[1], Zenjiro Sampei[1], Atsushi Muto[1], Tetsuo Kojima[1], Tetsuhiro Soeda[1], Kazutaka Yoshihashi[1], Yukiko Okuyama-Nishida[1], Hiroyuki Saito[1], Hiroyuki Tsunoda[1], Tsukasa Suzuki[1], Hideki Adachi[1], Taro Miyazaki[1], Shinya Ishii[1], Mika Kamata-Sakurai[1], Takeo Iida[1], Aya Harada[1], Keiko Esaki[1], Miho Funaki[1], Chifumi Moriyama[1], Eriko Tanaka[1], Yasufumi Kikuchi[1], Tetsuya Wakabayashi[1], Manabu Wada[1], Masaaki Goto[1], Takeshi Toyoda[1], Atsunori Ueyama[1], Sachiyo Suzuki[1], Kenta Haraya[1], Tatsuhiko Tachibana[1], Yoshiki Kawabe[1], Midori Shima[2], Akira Yoshioka[3] & Kunihiro Hattori[1]

Hemophilia A is a bleeding disorder resulting from coagulation factor VIII (FVIII) deficiency. Exogenously provided FVIII effectively reduces bleeding complications in patients with severe hemophilia A. In approximately 30% of such patients, however, the 'foreignness' of the FVIII molecule causes them to develop inhibitory antibodies against FVIII (inhibitors), precluding FVIII treatment in this set of patients[1–3]. Moreover, the poor pharmacokinetics of FVIII, attributed to low subcutaneous bioavailability and a short half-life of 0.5 d, necessitates frequent intravenous injections[3–5]. To overcome these drawbacks, we generated a humanized bispecific antibody to factor IXa (FIXa) and factor X (FX), termed hBS23, that places these two factors into spatially appropriate positions and mimics the cofactor function of FVIII. hBS23 exerted coagulation activity in FVIII-deficient plasma, even in the presence of inhibitors, and showed *in vivo* hemostatic activity in a nonhuman primate model of acquired hemophilia A. Notably, hBS23 had high subcutaneous bioavailability and a 2-week half-life and would not be expected to elicit the development of FVIII-specific inhibitory antibodies, as its molecular structure, and hence antigenicity, differs from that of FVIII. A long-acting, subcutaneously injectable agent that is unaffected by the presence of inhibitors could markedly reduce the burden of care for the treatment of hemophilia A.

About 1 in 10,000 males suffer from hemophilia A[6]. Approximately half of all patients with hemophilia A are classified as having severe disease[7], defined as <1% of normal FVIII activity, and such individuals typically experience at least one bleeding episode every month without preventive intervention[3,8]. Because patients with moderate hemophilia A (1–5% of normal activity) experience far fewer bleeding episodes, patients with severe disease are routinely given prophylactic supplementation of FVIII to keep the factor's activity to 1% or above, which effectively reduces joint bleeds, leading to better joint status and quality of life[3,8].

Despite these advantages, routine supplementation with FVIII has two major drawbacks aside from its expense: the development of inhibitors and the need for frequent venous access for FVIII injection. Inhibitors precluding the use of FVIII make it difficult to control hemorrhaging because alternative treatment agents (such as recombinant activated factor VII and activated prothrombin complex concentrates) have shorter half-lives, cost more than FVIII and are not always effective[9–11]. Eradication of inhibitors with high doses of FVIII is currently being attempted, but the process is very expensive and does not always work[12]. The need for frequent venous access is also problematic, particularly when treating pediatric patients at home[13], and it negatively affects both the implementation of and adherence to the supplementation routine. Therefore, a new agent that resolves these two drawbacks inherent to the current therapeutic use of FVIII has the potential to markedly improve the treatment possibilities for individuals with severe hemophilia A.

FVIII functions as a cofactor only when activated by either thrombin or factor Xa (FXa). The resultant factor VIIIa (FVIIIa) consists of the A1 subunit, the A2 subunit and the light chain (**Fig. 1a**)[14]. The light chain and the A2 subunit of FVIIIa respectively bind the light chain (K_d = 15 nM) and the heavy chain (K_d = 300 nM) of FIXa[15,16]. The A1 subunit of FVIIIa binds the heavy chain of FX (K_d = 1–3 μM)[17]. These binding properties contribute to FVIII's cofactor activity, enhancing the catalytic rate constant of FIXa and the interaction between FIXa and FX[14].

Recombinant monoclonal antibodies, with not only antagonistic activity but also agonistic[18], catalytic[19] or allosteric activity[20], have been extensively studied for their therapeutic applications[21]. Furthermore, bispecific antibodies, which recognize two different antigens, have been applied not only to simply neutralize two different antigens but also to recruit effector cells against the target cells[22] and to co-ligate two different antigens on the same cell[23]. We hypothesized that a bispecific IgG antibody recognizing FIXa with one arm and FX with the other could place FIXa and FX in spatially appropriate positions, as FVIIIa does, and promote FIXa-catalyzed FX activation (**Fig. 1b**).

[1]Fuji-Gotemba Research Laboratories, Chugai Pharmaceutical, Gotemba, Shizuoka, Japan. [2]Department of Pediatrics, Nara Medical University, Kashihara, Nara, Japan. [3]Nara Medical University, Kashihara, Nara, Japan. Correspondence should be addressed to T. Kitazawa (kitazawatkh@chugai-pharm.co.jp).

Received 11 May; accepted 16 August; published online 30 September 2012; doi:10.1038/nm.2942

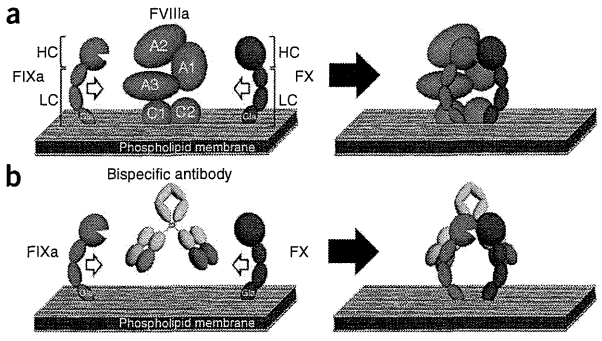

Figure 1 Schematic illustrations of the action of FVIIIa or of a bispecific antibody as a cofactor promoting the interaction between FIXa and FX. (**a**) FVIIIa consists of the A1 subunit, the A2 subunit and the light chain (A3, C1 and C2 subunits). FVIIIa forms a complex with FIXa and supports the interaction between FIXa and FX through its binding to both factors on the phospholipid membrane. HC, heavy chain; LC, light chain. (**b**) Bispecific antibody binding to FIXa and FX would promote the interaction between FIXa and FX on the phospholipid membrane and exert FVIII-mimetic activity. FVIIIa binds the phospholipid membrane via its C1 and C2 subunits; FIXa and FX bind the phospholipid membrane via their Gla domains. The illustrations describe the concept of the study only and do not necessarily indicate precise molecular structures and positions.

In support of this possibility, the distance between the FIXa- and FX-binding sites of FVIIIa[24] is similar to that between the two antigen-binding sites of human IgG[25]. In addition, antibody binding to the appropriate epitope of FIXa would mimic the allosteric properties of FVIIIa and enhance the catalytic activity of FIXa[14,16].

A bispecific antibody mimicking FVIII function could be an ideal agent for overcoming the two major drawbacks of current treatment. First, a bispecific antibody with a completely different molecular structure, or antigenicity, from FVIII would neither elicit inhibitors in patients with hemophilia A nor be neutralized by inhibitors that were already present. Moreover, humanized antibodies recently approved for clinical use have shown a low incidence of immunogenicity (<5%)[26]. Second, IgG antibodies have long plasma half-lives of 2 or 3 weeks and high subcutaneous bioavailability in humans, enabling once-a-month or less frequent treatment without venous access[27].

To create this type of bispecific antibody, we first generated various FIXa- and FX-specific monoclonal antibodies by immunizing animals with human FIXa and FX, respectively. We next used the genes encoding these monoclonal antibodies to generate bispecific IgG antibodies in which one arm would recognize FIXa and the other would recognize FX, as described in the Online Methods, and screened approximately 40,000 of these antibodies by an enzymatic assay for FX activation in the presence of FIXa and phospholipid. We identified a lead chimeric bispecific antibody with human IgG_4 heavy chain and κ light chain. Subsequent humanization and further engineering of the antibody generated an antibody termed hBS23. Surface plasmon resonance analysis showed that one of the arms of hBS23 recognizes factor IX (FIX) and FIXa, whereas the other arm recognizes FX and FXa (**Supplementary Fig. 1**). Western blotting analysis under reducing conditions showed that the epitope recognized by each arm of hBS23 is located in the FIXa light chain and the FX light chain, respectively (data not shown).

In an enzymatic assay using purified coagulation factors, hBS23 greatly enhanced FX activation, whereas monospecific one-armed antibodies[28] that had either the FIXa- or FX-specific variable region of hBS23 were completely inactive, as was a mixture of the two monospecific one-armed antibodies (**Fig. 2a**). hBS23 did not enhance FX activation in the absence of FIXa (**Fig. 2a**) or phospholipid (**Supplementary Fig. 2**), indicating that hBS23 functions as a cofactor mimicking FVIII and that the reaction required the presence of phospholipid. To compare the mechanistic basis for the cofactor function of hBS23 to that of FVIIIa, we performed a kinetic analysis of FIXa-catalyzed FX activation. Both hBS23 and FVIIIa increased the catalytic rate constant (k_{cat}) and decreased the Michaelis constant (K_m), consequently increasing the catalytic efficiency (k_{cat}/K_m) (**Table 1**). However, the extents to which they each affected k_{cat} and K_m were quite different; compared to FVIIIa, hBS23 showed ten times the effect on decreasing K_m, but 1/140th the effect on increasing k_{cat}, resulting in 1/14th the effect on increasing k_{cat}/K_m.

We next evaluated the activity of hBS23 in human FVIII-deficient plasma. With respect to the time to initiation of clot formation, hBS23 dose-dependently shortened the activated partial thromboplastin time (APTT) in FVIII-deficient plasma both in the presence and absence of inhibitors, whereas the effects of recombinant human FVIII (rhFVIII) on APTT were blocked by the presence of inhibitors (**Fig. 2b**). Doses of hBS23 greater than 30 nM had a greater effect on shortening the APTT compared to 1 U ml^{-1} rhFVIII (100% of normal FVIII activity). The shorter APTT achieved by hBS23 compared to that under normal FVIII activity can be explained by the fact that FVIII requires additional time to be activated by thrombin or FXa, whereas hBS23 does not. To further examine the therapeutic potential of hBS23, we evaluated its effect on thrombin burst in a thrombin generation assay (TGA)[29] in human FVIII-deficient plasma. hBS23 dose-dependently improved thrombin generation parameters, including peak height (defined as the peak of free thrombin concentration) and endogenous thrombin potential (ETP, defined as the area under the curve, a readout of the overall capacity of plasma to form thrombin) even in the presence of inhibitors that rendered rhFVIII completely ineffective (**Fig. 2c–e** and **Supplementary Fig. 3**). With respect to peak height, hBS23 exerted activity equivalent to 0.01 U ml^{-1} (1%) rhFVIII at a concentration of ~30 nM and equivalent to nearly 0.1 U ml^{-1} (10%) rhFVIII at a concentration of ~300 nM. These results suggest that hBS23 has the potential to exert sufficient FVIII-mimetic activity for routine prophylactic use, even in patients with inhibitors who are nonresponsive to FVIII treatment.

To evaluate the *in vivo* hemostatic activity of hBS23, which is highly species specific in the manner in which it exerts FVIII-mimetic activity, we needed a hemophilia A model in nonhuman primates. As nonhuman primates with inherited hemophilia A were unavailable, we established an acquired hemophilia A model. For this purpose, we identified a neutralizing antibody against FVIII from mice, termed VIII-2236, which was cross-reactive to cynomolgus monkey FVIII but not to porcine FVIII (**Supplementary Fig. 4**). Injection of VIII-2236 into cynomolgus monkeys neutralized endogenous FVIII (data not shown) but not exogenous recombinant porcine FVIII (rpoFVIII). We established hemophilia A status by injecting cynomolgus monkeys with VIII-2236 and then artificially induced bleeding (**Fig. 3a**). The monkeys in the control group showed progressive anemia (as assessed by a decrease in hemoglobin levels) and an expanded bruised area (**Fig. 3b,c**). Compared to the control, bolus intravenous administration of 0.3 mg per kg body weight of hBS23 significantly prevented the decrease in hemoglobin levels ($P = 0.0116$) and tended to reduce the bruised area ($P = 0.0522$). This hemostatic activity of hBS23 was comparable to that of twice-daily intravenous administration of 1 U per kg body weight of rpoFVIII (**Fig. 3b,c**), which would